Studying Azobenzene-Modified DNA for Programmable Nanoparticle Assembly and Nucleic Acid Detection

Yunqi Yan

A dissertation
submitted in partial fulfilment of the
requirements for the degree of

Doctor of Philosophy

University of Washington
2015

Reading Committee
David Ginger, Chair
Daniel Chiu
Lutz Maibaum

Program Authorized to Offer Degree:
Chemistry

University of Washington

Abstract

Studying Azobenzene-Modified DNA for Programmable Nanoparticle Assembly and Nucleic Acid Detection

Yunqi Yan

Chair of the Supervisory Committee: Professor David Ginger
Department of Chemistry

The azobenzene-modified DNA is an oligonucleotide molecule with azobenzene moieties covalently linked to the DNA backbone via the d-threoninol bond. The reversible photoswitching capability of azobenzene allows optical irradiation (light) to control the hybridization of azobenzene-modified DNA. Meanwhile, gold nanoparticles functionalized with natural oligonucleotides show increased sensitivity in nucleic acid detection due to the DNA-directed biorecognition and nanoparticles' plasmonic effects. In the dissertation, I present my studies of surface functionalization of gold nanoparticles with azobenzene-modified oligonucleotides and the relevant photochemical characterization of the new system.

In chapter 2, I synthesize the photoswichable gold nanoparticle assemblies cross-linked with azobenzene-modified DNA. Beyond the classic DNA-directed assembly and sensing behaviors associated with DNA-modified nanoparticles, these particles exhibit reversible photoswitching of their assembly behavior. Exposure to UV light induces the dissociation of nanoparticle aggregates due to *trans-to-cis* isomerization of the azobenzene which destabilizes the DNA duplex. The assembly of nanoparticles is reversible upon exposure to blue light due to the reverse *cis-to-trans* isomerization of azobenzene-modified DNA. I further find that perfectly complementary and partially mismatched strands exhibit clearly distinguishable photoinduced melting properties, and I demonstrate that photon dose can thus be used in place of temperature

or ionic strength to control hybridization stringency with the ability to discriminate single-base mismatches.

In chapter 3, I study the sequence dependence of the photoinduced isomerization quantum yield of azobenzene-modified DNA. Compared to the free azobenzene, the *trans-to-cis* isomerization quantum yield is decreased 3-fold (from 0.094 ± 0.004 to 0.036 ± 0.002) when the azobenzene is incorporated into single-strand DNA (ssDNA), and is further reduced 15-fold (to 0.0056 ± 0.0008) for azobenzene incorporated into double-strand DNA (dsDNA). Quantum yield is also sensitive to the local sequence including both specific mismatches and the overall sequence-dependent melting temperature.

In chapter 4, I study hybridization and light-induced dehybridization of azobenzene-modified DNA bound to glass substrates with fluorescently-labeled oligonucleotide targets in solution. I show that fluorescent readout using a commercial array scanner is compatible with azobenzene-modified DNA capture sequences. In addition, I demonstrate that I can photoswitch azobenzene molecules on a surface in the presence of fluorophores and thus that I am able to control the dehybridization behavior of the immobilized azobenzene-modified DNA with its target sequence in solution. I further study the dehybridization of perfectly-matched target sequences and the single-base-mismatched sequences as a function of radiant fluence. I measure lower fluorescent signals for sequences with a single-base mismatch than that for perfectly-matched sequences, showing that mismatched sequences dehybridized more efficiently upon UV illumination. The extension of this photoinduced differential dehybridization phenomenon to surfaces in the presence of fluorophores indicates that optical DNA hybridization stringency is compatible with chip-based applications for heterogeneous assays.

TABLE OF CONTENTS

LIST OF FIGURES

LIST OF TABLES

Acknowledgements

First and foremost, I would like to acknowledge my parents. I own all my achievements to my parents. Mom and Dad have brought me up with the best opportunities they could provide. Mom has encouraged me to pursue education abroad and has supported me emotionally ever since. I am writing the thesis during the hard time when Dad and Mon are struggling with the diseases. I am regretful that I am unable to support Mom and Dad as they have done for me. I wish all the best to them.

我想真挚地感谢我的父母亲为这篇论文所做出的贡献。随着我的成长，我体会到，妈妈和爸爸在抚养我的过程中付出了他们最大的努力。我还能记得，妈妈曾经鼓励去外地求学，去国外求学。在这 10 年的求学中，妈妈在精神和情感上也给予了我很多支持。在我写这篇论文的时候，也是我父母非常困难的时候。爸爸受病魔受苦，父母一起和疾病做着斗争。我感到非常遗憾无法给予他们同等的支持和帮助。我希望爸爸妈妈能够渡过这次难关，平平安安，健健康康。我将这篇论文和我求学所获得的成就，都献给他们。我想用这首古诗，来表达我对父母的感谢，以及我万般无奈无法陪伴父母的心情。

慈母手中线，游子身上衣，临行密密缝，意恐迟迟归，谁言寸草心，抱得三春晖。

I would like to acknowledge a lot of people for the completion of the dissertation. I want to thank my advisor Prof. David Ginger who has been so patiently guided me how to do scientific researches. He has supported me with a wealth of opportunities and has provided suggestions that will benefit me long way after graduate school. Thank you! I could not achieve what I have covered in the dissertation without your support.

I want to give my dedication to the whole Ginger lab for being great co-workers. Thanks to Dr. Jennifer Chen who has trained me hand-by-hand from scratch in the lab. She has helped me with the photoswitching experiments and the darkfield microscopy experiments. Her serious

attitude with scientific data and her generosity to help members in the lab has inspired me throughout my research in graduate school. Thanks go to Dr. Keiko Munechika, Dr. Xin Wang and Dr. Esha Sengupta for showing me the AFM experiments and AFM data analysis. I could not reach my research achievements without all of your help.

I am very thankful for my collaborators. Discussions with Adelaide Kingsland from Prof. Lutz Maibaum group has helped me futher understand the "free volume" mechanism that we have proposed in chapter 3. Dr. Lucas Parents and Dr. James Evans at the Pacific Northwestern National Laboratory have showed me the advanced design of liquid cells that allow liquid samples to be tested with the TEM. Many thanks to Dr. Jennifer McCullar and Dr. Andrew Laughlin at C4C who have patiently educated me with patent and commercialization knowledge.

Finally, I would like acknowledge AFOSR and UW C4C for funding my research projects.

Chapter I Background and Motivation

1.1 Azobenzene and photo-induced isomerization

Azobenzene, a phenyl derivative of diazene family (Figure 1.1a), has two configurations—the trans-azobenzene[1] and the cis-azobenzene that Hartley[2,3] had isolated 80 years ago. Trans-azobenzene is a planar molecule with zero dipole moment. X-ray data[4,5] indicates that CNNC dihedral angle is 180° and CNN angle is 114°.[6] Cis-azobenezenen, with 3-Debye dipole moment,[7] is a non-planar molecule with CNNC dihedral angle being 172° and phenyl group twist angle being 53°.[8] Azobenzene has unique photoswitching property that trans-azobenzene isomerizes to cis-azobenzene under UV irradiation (~300-370 nm) and cis-azobenzene converts to trans-azobenzene upon blue irradiation (~430-460 nm) or heat.(Figure 1.1a) This trans-to-cis photoswitching is almost completely reversible because azobenzene is photo-stable.[9] No photo-induced decomposition happens after prolonged irradiation time,[10] and the trans-form to cis-form ratio stays unchanged after photo-stationary state achieves.[11]

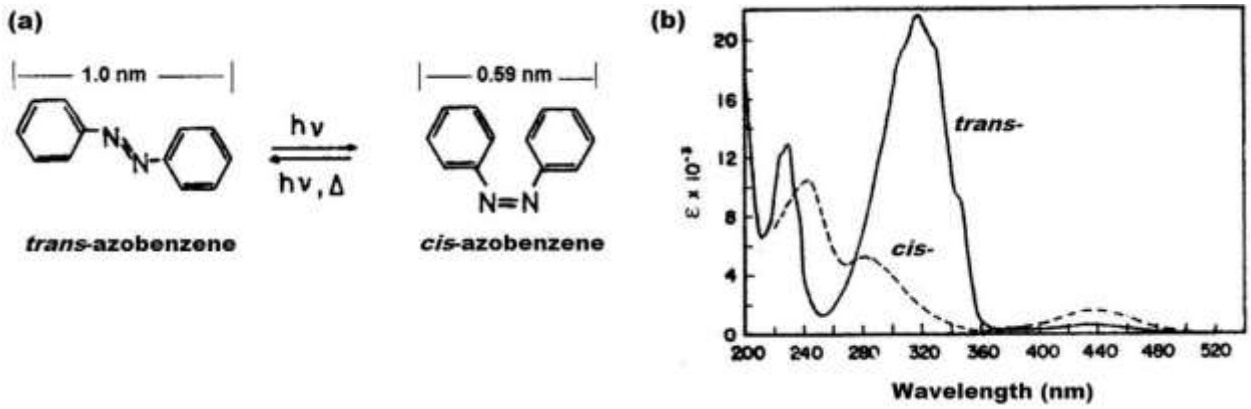

Figure 1.1 Structural and electronic features of azobenzene molecules.

(a) Photo-isomerization of trans-azobenzene and cis-azobenzene; (b) Optical extinction coefficient spectra of trans-azobenzene and cis-azobenzene in ethanol. (Image is preprinted with permission of reference 10 Copyright Elsevier Science.)

Trans-azobenzene and cis-azobenzene have unique absorption spectroscopy features that affect their photo-isomerization reactions. Figure1.1b shows the plot of the absorption coefficient versus wavelength for azobenzene molecules.[10] Notably, trans-azobenzene has its main absorption band maximized at 330 nm with absorption coefficient being ~22000 L/mol/cm).[12] It is reported that the π-to-π* electronic transition of the nitrogen atoms is responsible for 330 nm absorption in the UV region. Meanwhile, trans-azobenzene has a weaker absorption band in the visible region centered at ~450 nm with absorption coefficient being ~400 L/mole/cm.[13] This blue absorption at 450 nm corresponds to the n-to-π* electronic transition which virtually requires lower energy.

Cis-azobenzene has a weaker π-to-π* electronic transition and shows absorption feature in the UV region centered at ~240 nm (11000 L/mol/cm) and ~280 nm (5000 L/mol/cm).[10] The n-to-π* transition of cis-azobenzene absorbs energy at ~450 nm (1500 L/mol/cm)[9] and exhibits a relatively stronger absorption than that of trans-azobenzene at the same wavelength.

Photo-induced isomerization happens in both directions under optical irradiation from trans-form to cis-form and from cis-form to trans-form. The thermal-induced cis-to-trans isomerization is usually negligible because it is slow at room temperature with a half-life time being 2-3 days.[14,15] In order to quantify the photonic efficiency of the photo-isomerization reaction, quantum yield (QY) is measured as an important parameter. There are two types of QY: the trans-to-cis isomerization QY and the cis-to-trans QY. This dissertation focuses on discussions of trans-to-cis QY in chapter 3. The trans-to-cis QY is defined and calculated as the ratio of "the number of isomerized trans-azobenzene" to "the number of absorbed photons" at the irradiation wavelength and at the incident time.[10,11]

The trans-to-cis QY depends on the irradiation wavelength such that the QY reduces at high-energy irradiation (shorter wavelength), whereas the QY increase at low-energy irradiation (longer wavelength).[16-18] For example, Zimmerman et al measured the trans-to-cis QY being ~0.1 for 365 nm UV irradiation and being ~0.4 for 450 nm blue irradiation.[11] Other conditions like solution viscosity[19,20] and azobenzene molecular substitution[21] affect the trans-to-cis isomerization QY.

The kinetics of photo-isomerization reactions can be monitored by spectroscopy features of azobenzene molecules. The following rate equation describes the reaction:[11,22]

$$\frac{d[cis]_t}{dt} = \frac{I * l * \left(1 - 10^{-abs(t)}\right) * \phi_{trans} * \varepsilon_{trans}}{V * abs(t)} \left([trans]_0 - [cis]_t\right)$$

$$- \frac{I * l * \left(1 - 10^{-abs(t)}\right) * \phi_{cis} * \varepsilon_{cis}}{V * abs(t)} [cis]_t$$

where $[cis]_t$ is the concentration of *cis*-azobenzene at time t; $[trans]_0$ is concentration of *trans*-azobenzene before photoisomerization which is assumed to be the total concentration of azobenzene; I is the intensity of the excitation; l is the beam path length of UV-vis absorption measurement; $abs(t)$ is the absorbance of the sample at the excitation wavelength, and t is time; ϕ_{trans} and ϕ_{cis} are the quantum yields of *trans*-to-*cis* and *cis*-to-*trans* isomerization; ε_{trans} and ε_{cis} are the absorption coefficients at the excitation wavelength of *trans*-azobenzene and *cis*-azobenzene; V is the volume. There will be more explanations in chapter 5.

Photo-induced isomerization reaction at 315 nm reaches its photo-stationary state with more than 90% of trans-azobenzene converting to cis-azobenzene.[22,23] The fraction of cis-azobenzene at photo-stationary state also depends on irradiation wavelength. In the recent 20 years, ultrafast time-resolved spectroscopy techniques have enabled measurement of short-lived

excited states of trans-azobenzene and cis-azobenzene, answering questions of photo-isomerization kinetics in ultrafast time scale.[24-26]

The trans-to-cis isomerization mechanism is also a hot topic that is under investigation using advanced experimental[24] and simulation[27] methods. The following two pathways[28,29]—rotation and inversion—are in the center among all other mechanism.(Figure 1.2) Studies support that the UV-induced trans-to-cis isomerization (S2 ← S0) tends to follow the rotation pathway; while the blue-induced trans-to-cis isomerization (S1 ← S0) favors the inversion mechanism. More recent studies have proposed new mechanisms based on the rotation and inversion such as converted inversion and inversion-assisted rotation.[9]

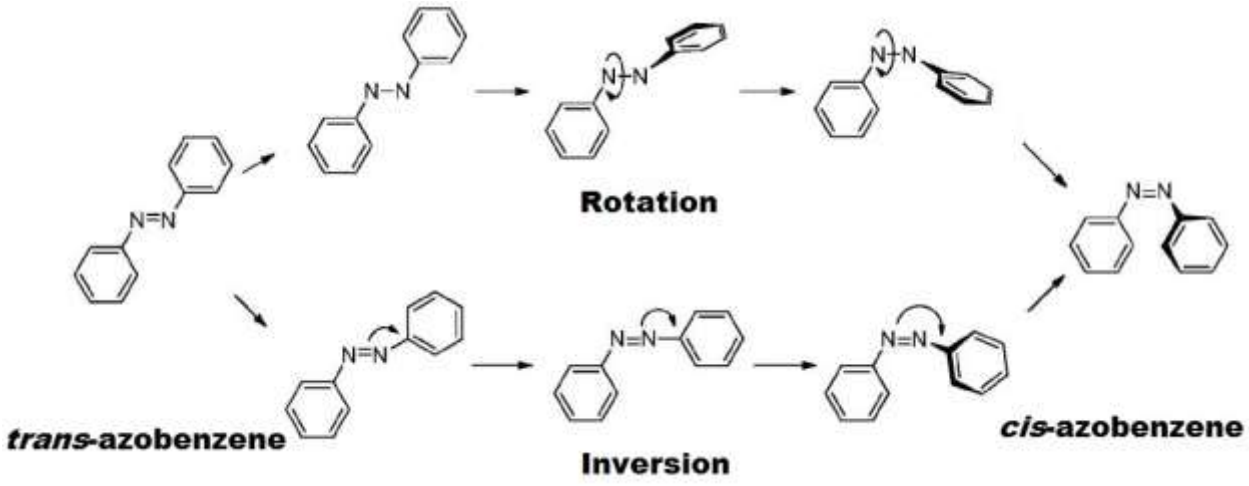

Figure 1.2 Trans-to-cis photoisomerization mechanism.
(Image is reprinted with permission of reference 9.) Copyright RSC Publishing.

1.2 Azobenzene-modified DNA

Azobenzene has been embedded via chemical methods to many light-inert systems such as small molecules,[30-34] polymers,[35-37] and proteins.[38-40] The motivation beneath azobenzene modification is to create a photo-reactive system whose functionality is manipulated by optical

triggers via photo-isomerization of azobenzene units.[41,42] Virtually, azobenzene is a good candidate to be coupled to proteins, DNAs or RNAs to create a photo-responsive system because the azobenzene-modified system is fully reversible with no side reactions.[10]

Asanuma research group has pioneered in synthesizing and characterizing azobenzene-modified DNA.[43,44] Using azobenzene-modified phosphoramidate precursor in the DNA synthesizer,[45] Asanuma et al successfully synthesized azobenzene-modified oligonucleotide that bear multiple azobenzene units[46] in the backbone via d-threoninol covalent linkage (Figure 1.3). Despite some structural distortion resulting from extra volume of azobenzene moieties,[47] the modified single-stranded DNA (ssDNA) is able to form double-stranded (dsDNA) with its complementary sequence.[48]

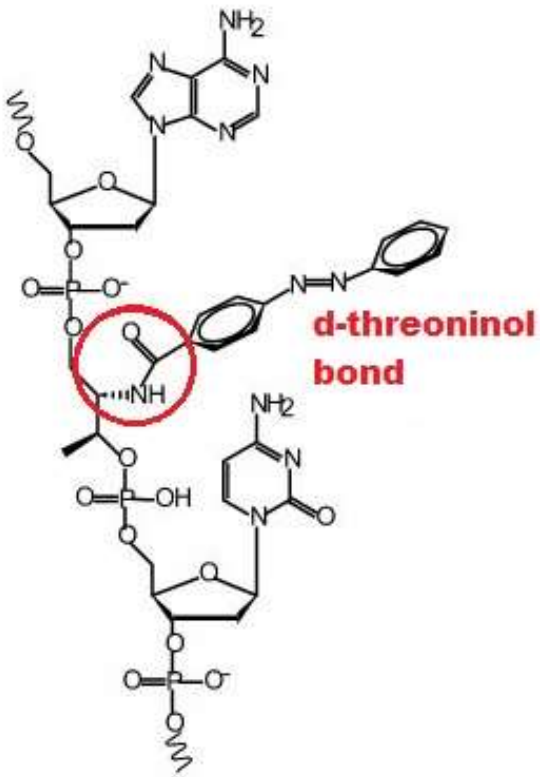

Figure 1.3 Chemical structure of the d-threoninol bond in azobenzene-modified DNA.

It is discovered that the trans-azobenzene stabilizes the dsDNA as the melting temperature of azobenzene-modified (in trans-form) duplex is measured with an increased value than that of unmodified duplex.[48] NMR studies[47] show that phenyl groups of the trans-azobenzene form π-π stacking interaction with the nearby nucleotide bases, which increases the stability of dsDNA. However, when trans-azobenzene isomerizes to its cis-form upon UV irradiation, the π-π electronic interaction disappears and the steric hindrance appears. The cis-azobenzene, with a reduced melting temperature relative to the corresponding unmodified duplex, cause the dsDNA to dehybridize into ssDNA.[49] Furthermore, the dehybridized ssDNA is able to rehybridize to dsDNA when blue irradiation reverse the isomerization reaction by converting cis-azobenzene to the trans-form.[50] As a result, the hybridization and dehybridization of azobenzene-modified DNA are controlled in a fully-reversible manner by optical irradiation, when other factors such as temperature and buffer concentration are maintained the same. Azobenzene-modified DNA has been studied for applications including control of genetic expression,[51-53] photo-driven DNA nanomotors,[54-56] enzyme inhibition[39,57] and so on.

1.3 DNA-functionalized gold nanoparticles

Gold nanoparticles covalently functionalized with a dense layer of oligonucleotides[58] are widely studied for their unique properties,[59-61] which are markedly different from gold nanoparticle and DNA. Gold nanoparticles exhibit localized surface plasmon resonances[62] (LSPRs) that are sensitive to nanoparticle's size and shape,[63] refractive index[64] and interparticle coupling.[65,66] The LSPR contributes to the physical and chemical characteristics of gold nanoparticle such as the strong catalytic ability[67-69] and improved light scattering efficiency.[70-72] Densely-coated oligonucleotides on gold nanoparticle surface,[73] in addition to its usually base-

pairing recognition feature, add new characteristics such as increased stability[74,75] and sharp dissociation transition[76] to the newly-created DNA-functionalized gold nanoparticles.

Oligonucleotides bear three unique regions—the thiolate end, the spacer and the base-pairing region.(see Figure 2.1) The thiolate region at either 5' or 3' end of the oligonucleotide is covalently modified with a hexylthiol group, forming Au-S bond[77-79] that enables covalent attachment of oligonucleotides to gold nanoparticles. The spacer region aims to physically separate the gold nanoparticle core and the base-paring region by consisting of 10-30 poly-adenine (polyA) or poly-thymine (polyT). The base-pairing region contains well-designed DNA sequences that are able to hybridize with their complementary oligonucleotides. It is the active and functional region of the oligonucleotide that can be tailored for applicable purposes. Virtually, the base-pairing region can be built in a DNA synthesizer with chemically-altered nucleotides via the advancement of phosphoramidite chemistry.[80,81] This dissertation will discuss the azobenzene-modified "artificial base" embedded for the DNA-functionalized gold nanoparticle system.

In 1996, Mirkin et al successfully created DNA-functionalized gold nanoparticles by using 8-nucleotide thiolated oligonucleotides with 15-nm gold nanoparticles.[58] The group achieved high density loading of oligonucleotides on the surface of gold nanoparticles[82] with the coverage being ~10^{13} DNA/cm^2.[73] It was challenging to functionalize oligonucleotides on nanoparticle surfaces in a densely-packing manner because oligonucleotides are negative charged in the backbone, and thus repel neighboring strands. The Mirkin group developed a synthetic method to gradually screen the repulsive electrostatic force by step-wisely increasing the sodium ion concentration, a method that they name it salt-aging.[82] They also discovered that

sonication and elevated temperature help increase the packing density of DNA molecules on nanoparticles.[83] I adapted most of their methods in chapter 2.

Single nanoparticles form large nanoparticle assemblies because of the hybridization between complementary DNA that are coated on nanoparticle surface. Immobilized oligonucleotides exhibit increased binding affinity to complementary DNA strands[84] with increased dehybridization temperature (also called "melting temperature") compared to that of free unmodified DNA.[76] The thermal-induced dehybridization exhibit a sharper and narrower transition compared to that of free DNAs,[59] allowing DNA-nanoparticle conjugates being extremely sensitive to detect even a single-base mismatch in DNA sequence.[82,85,86]

Mirkin and Schatz groups[76] have explored experimental and theoretical approaches to study the increased and sharper DNA melting behavior when DNA molecules are heavily functionalized on the nanoparticle surface. They discovered two factors—the dense coverage of surface-coated oligonucleotides and the high local sodium ion concentration around oligonucleotides[87] —that make oligonucleotide interact more collectively with the neighboring strands in close proximity. The collective and strong interactions give rise to higher effective oligonucleotide concentration, and thus result in higher melting temperature and sharper melting transition.

DNA-functionalized gold nanoparticle conjugates have demonstrated applications in programmable assembly of complex nanostructures,[88-91] biological sensing,[92,93] and gene regulation,[94,95] The assembly and binding properties of DNA-functionalized nanoparticles have been controlled primarily by chemical reagents (e.g. the presence of complementary DNA sequences or aptamer targets[96]) or by classical inputs that affect DNA hybridization such as salt concentration or temperature. Conferring DNA-nanoparticle conjugates with additional stimulus-

response behavior could open many opportunities for new diagnostic, sensing, and nanofabrication applications by enabling the reversible triggering of DNA-directed nanoparticle assembly and associated optical responses.

In the dissertation, I seek to confer such stimulus-response functionality to these versatile materials by functionalizing gold nanoparticles with azobenzene-modified DNA.

1.4 References

(1) Adamson, A. W.; Vogler, A.; Kunkely, H.; Wachter, R. *Journal of the American Chemical Society* **1978**, *100*, 1298-1300.

(2) Hartley, G. S. *Nature* **1937**, *140*, 281-281.

(3) Hartley, G. S. *Journal of the Chemical Society* **1938**, 633-642.

(4) Bouwstra, J. A.; Schouten, A.; Kroon, J. *Acta Crystallographica Section C-Crystal Structure Communications* **1983**, *39*, 1121-1123.

(5) de Lange, J. J.; Robertson, J. M.; Woodward, I. *Proceedings of the Royal Society of London Series a-Mathematical and Physical Sciences* **1939**, *171*, 0398-0410.

(6) Traetteberg, M.; Hilmo, I.; Hagen, K. *Journal of Molecular Structure* **1977**, *39*, 231-239.

(7) Fliegl, H.; Kohn, A.; Hattig, C.; Ahlrichs, R. *Journal of the American Chemical Society* **2003**, *125*, 9821-9827.

(8) Hampson, G. C.; Robertson, J. M. *Journal of the Chemical Society* **1941**, 409-413.

(9) Bandara, H. M.; Burdette, S. C. *Chem Soc Rev* **2012**, *41*, 1809-1825.

(10) Rau, H. In *Photoreactive Organic Thin Films*, Sekkat, Z.; Kroll, W., Eds.; Elsevier Incorporation, 2002, pp 3-47.

(11) Zimmerman, G.; Chow, L. Y.; Paik, U. J. *Journal of the American Chemical Society* **1958**, *80*, 3528-3531.

(12) Forber, C. L.; Kelusky, E. C.; Bunce, N. J.; Zerner, M. C. *Journal of the American Chemical Society* **1985**, *107*, 5884-5890.

(13) Hochstrasser, R. M.; Lower, S. K. *Journal of Chemical Physics* **1962**, *36*, 3505-&.

(14) Andersson, J. A.; Petterson, R.; Tegner, L. *Journal of Photochemistry* **1982**, *20*, 17-32.

(15) Talaty, E. R.; Fargo, J. C. *Chemical Communications* **1967**, 65-&.

(16) Yamashita, S.; Ono, H.; Toyama, O. *Bulletin of the Chemical Society of Japan* **1962**, *35*, 1849-1853.

(17) Siampiringue, N.; Guyot, G.; Monti, S.; Bortolus, P. *Journal of Photochemistry* **1987**, *37*, 185-188.

(18) Ronayett.J; Arnaud, R.; Lebourge.P; Lemaire, J. *Canadian Journal of Chemistry-Revue Canadienne De Chimie* **1974**, *52*, 1848-1857.

(19) Bortolus, P.; Monti, S. *Journal of Physical Chemistry* **1979**, *83*, 648-652.

(20) Gegiou, D.; Muszkat, K. A.; Fischer, E. *Journal of the American Chemical Society* **1968**, *90*, 12-&.

(21) Gegiou, D.; Muszkat, K. A.; Fischer, E. *Journal of the American Chemical Society* **1968**, *90*, 3907-&.

(22) Yan, Y. Q.; Wang, X.; Chen, J. I. L.; Ginger, D. S. *Abstr Pap Am Chem S* **2014**, *248*.

(23) Fischer, E. *Journal of the American Chemical Society* **1960**, *82*, 3249-3252.

(24) Fujino, T.; Arzhantsev, S. Y.; Tahara, T. *Journal of Physical Chemistry A* **2001**, *105*, 8123-8129.

(25) Chang, C. W.; Lu, Y. C.; Wang, T. T.; Diau, E. W. G. *Journal of the American Chemical Society* **2004**, *126*, 10109-10118.

(26) Lednev, I. K.; Ye, T. Q.; Matousek, P.; Towrie, M.; Foggi, P.; Neuwahl, F. V. R.; Umapathy, S.; Hester, R. E.; Moore, J. N. *Chemical Physics Letters* **1998**, *290*, 68-74.

(27) Crecca, C. R.; Roitberg, A. E. *Journal of Physical Chemistry A* **2006**, *110*, 8188-8203.

(28) Rau, H.; Luddecke, E. *Journal of the American Chemical Society* **1982**, *104*, 1616-1620.

(29) Rau, H. *Journal of Photochemistry* **1984**, *26*, 221-225.

(30) Ferri, V.; Elbing, M.; Pace, G.; Dickey, M. D.; Zharnikov, M.; Samori, P.; Mayor, M.; Rampi, M. A. *Angewandte Chemie-International Edition* **2008**, *47*, 3407-3409.

(31) Wen, Y. Q.; Yi, W. H.; Meng, L. J.; Feng, M.; Jiang, G. Y.; Yuan, W. F.; Zhang, Y. Q.; Gao, H. J.; Jiang, L.; Song, Y. L. *Journal of Physical Chemistry B* **2005**, *109*, 14465-14468.

(32) Muraoka, T.; Kinbara, K.; Aida, T. *Nature* **2006**, *440*, 512-515.

(33) Evangelio, E.; Saiz-Poseu, J.; Maspoch, D.; Wurst, K.; Busque, F.; Ruiz-Molina, D. *European Journal of Inorganic Chemistry* **2008**, 2278-2285.

(34) Gorostiza, P.; Isacoff, E. Y. *Science* **2008**, *322*, 395-399.

(35) Bang, C. U.; Shishido, A.; Ikeda, T. *Macromolecular Rapid Communications* **2007**, *28*, 1040-1044.

(36) Puntoriero, F.; Ceroni, P.; Balzani, V.; Bergamini, G.; Vogtle, F. *Journal of the American Chemical Society* **2007**, *129*, 10714-10719.

(37) Parker, R. M.; Gates, J. C.; Rogers, H. L.; Smith, P. G. R.; Grossel, M. C. *Journal of Materials Chemistry* **2010**, *20*, 9118-9125.

(38) Banghart, M. R.; Mourot, A.; Fortin, D. L.; Yao, J. Z.; Kramer, R. H.; Trauner, D. *Angewandte Chemie-International Edition* **2009**, *48*, 9097-9101.

(39) Kim, Y. M.; Phillips, J. A.; Liu, H. P.; Kang, H. Z.; Tan, W. H. *Proceedings of the National Academy of Sciences of the United States of America* **2009**, *106*, 6489-6494.

(40) Wang, J.; Liu, H. B.; Ha, C. S. *Tetrahedron* **2009**, *65*, 9686-9689.

(41) Beharry, A. A.; Woolley, G. A. *Chemical Society Reviews* **2011**, *40*, 4422-4437.

(42) Barrett, C. J.; Mamiya, J. I.; Yager, K. G.; Ikeda, T. *Soft Matter* **2007**, *3*, 1249-1261.

(43) Asanuma, H.; Ito, T.; Komiyama, M. *Tetrahedron Letters* **1998**, *39*, 9015-9018.

(44) Asanuma, H.; Liang, X.; Nishioka, H.; Matsunaga, D.; Liu, M.; Komiyama, M. *Nature Protocols* **2007**, *2*, 203-212.

(45) Asanuma, H.; Yoshida, T.; Ito, T.; Komiyama, M. *Tetrahedron Letters* **1999**, *40*, 7995-7998.

(46) Asanuma, H.; Matsunaga, D.; Komiyama, M. *Nucleic Acids Symposium Series* **2005**, 35-36.

(47) Liang, X. G.; Asanuma, H.; Kashida, H.; Takasu, A.; Sakamoto, T.; Kawai, G.; Komiyama, M. *Journal of the American Chemical Society* **2003**, *125*, 16408-16415.

(48) Liang, X. G.; Mochizuki, T.; Asanuma, H. *Small* **2009**, *5*, 1761-1768.

(49) Asanuma, H.; Ito, T.; Yoshida, T.; Liang, X. G.; Komiyama, M. *Angewandte Chemie-International Edition* **1999**, *38*, 2393-2395.

(50) Asanuma, H.; Liang, X. G.; Yoshida, T.; Komiyama, M. *Chembiochem* **2001**, *2*, 39-44.

(51) Matsunaga, D.; Asanuma, H.; Komiyama, M. *Journal of the American Chemical Society* **2004**, *126*, 11452-11453.

(52) Liu, M. Z.; Asanuma, H.; Komiyama, M. *Journal of the American Chemical Society* **2006**, *128*, 1009-1015.

(53) Lee, S. E.; Liu, G. L.; Kim, F.; Lee, L. P. *Nano Letters* **2009**, *9*, 562-570.

(54) Kang, H. Z.; Liu, H. P.; Phillips, J. A.; Cao, Z. H.; Kim, Y.; Chen, Y.; Yang, Z. Y.; Li, J. W.; Tan, W. H. *Nano Letters* **2009**, *9*, 2690-2696.

(55) McCullagh, M.; Franco, I.; Ratner, M. A.; Schatz, G. C. *Journal of the American Chemical Society* **2011**, *133*, 3452-3459.

(56) Liang, X. G.; Nishioka, H.; Takenaka, N.; Asanuma, H. *Chembiochem* **2008**, *9*, 702-705.

(57) You, M. X.; Wang, R. W.; Zhang, X. B.; Chen, Y.; Wang, K. L.; Peng, L.; Tan, W. H. *Acs Nano* **2011**, *5*, 10090-10095.

(58) Mirkin, C. A.; Letsinger, R. L.; Mucic, R. C.; Storhoff, J. J. *Nature* **1996**, *382*, 607-609.

(59) Rosi, N. L.; Mirkin, C. A. *Chemical Reviews* **2005**, *105*, 1547-1562.

(60) Tan, S. J.; Campolongo, M. J.; Luo, D.; Cheng, W. L. *Nature Nanotechnology* **2011**, *6*, 268-276.

(61) Cutler, J. I.; Auyeung, E.; Mirkin, C. A. *Journal of the American Chemical Society* **2012**, *134*, 1376-1391.

(62) Willets, K. A.; Van Duyne, R. P. In *Annual Review of Physical Chemistry*, 2007, pp 267-297.

(63) Link, S.; El-Sayed, M. A. *Journal of Physical Chemistry B* **1999**, *103*, 4212-4217.

(64) Underwood, S.; Mulvaney, P. *Langmuir* **1994**, *10*, 3427-3430.

(65) Sonnichsen, C.; Reinhard, B. M.; Liphardt, J.; Alivisatos, A. P. *Nature Biotechnology* **2005**, *23*, 741-745.

(66) Jain, P. K.; Huang, W. Y.; El-Sayed, M. A. *Nano Letters* **2007**, *7*, 2080-2088.

(67) Heddle, J. G. *Catalysts* **2013**, *3*, 683-708.

(68) Panigrahi, S.; Basu, S.; Praharaj, S.; Pande, S.; Jana, S.; Pal, A.; Ghosh, S. K.; Pal, T. *Journal of Physical Chemistry C* **2007**, *111*, 4596-4605.

(69) Gong, J. L.; Mullins, C. B. *Accounts of Chemical Research* **2009**, *42*, 1063-1073.

(70) Dasary, S. S. R.; Singh, A. K.; Senapati, D.; Yu, H. T.; Ray, P. C. *Journal of the American Chemical Society* **2009**, *131*, 13806-13812.

(71) Alexander, K. D.; Hampton, M. J.; Zhang, S. P.; Dhawan, A.; Xu, H. X.; Lopez, R. *Journal of Raman Spectroscopy* **2009**, *40*, 2171-2175.

(72) Qian, X. M.; Nie, S. M. *Chemical Society Reviews* **2008**, *37*, 912-920.

(73) Hill, H. D.; Millstone, J. E.; Banholzer, M. J.; Mirkin, C. A. *Acs Nano* **2009**, *3*, 418-424.

(74) Leff, D. V.; Brandt, L.; Heath, J. R. *Langmuir* **1996**, *12*, 4723-4730.

(75) Giljohann, D. A.; Seferos, D. S.; Patel, P. C.; Millstone, J. E.; Rosi, N. L.; Mirkin, C. A. *Nano Letters* **2007**, *7*, 3818-3821.

(76) Jin, R. C.; Wu, G. S.; Li, Z.; Mirkin, C. A.; Schatz, G. C. *Journal of the American Chemical Society* **2003**, *125*, 1643-1654.

(77) Hakkinen, H. *Nature Chemistry* **2012**, *4*, 443-455.

(78) Pensa, E.; Cortes, E.; Corthey, G.; Carro, P.; Vericat, C.; Fonticelli, M. H.; Benitez, G.; Rubert, A. A.; Salvarezza, R. C. *Accounts of Chemical Research* **2012**, *45*, 1183-1192.

(79) Chen, I. W. P.; Chen, C. C.; Lin, S. Y.; Chen, C. H. *Journal of Physical Chemistry B* **2004**, *108*, 17497-17504.

(80) Benner, S. A. *Accounts of Chemical Research* **2004**, *37*, 784-797.

(81) Venkatesan, N.; Kim, S. J.; Kim, B. H. *Current Medicinal Chemistry* **2003**, *10*, 1973-1991.

(82) Elghanian, R.; Storhoff, J. J.; Mucic, R. C.; Letsinger, R. L.; Mirkin, C. A. *Science* **1997**, *277*, 1078-1081.

(83) Hurst, S. J.; Lytton-Jean, A. K. R.; Mirkin, C. A. *Analytical Chemistry* **2006**, *78*, 8313-8318.

(84) Lytton-Jean, A. K. R.; Mirkin, C. A. *Journal of the American Chemical Society* **2005**, *127*, 12754-12755.

(85) Taton, T. A.; Mirkin, C. A.; Letsinger, R. L. *Science* **2000**, *289*, 1757-1760.

(86) Taton, T. A.; Lu, G.; Mirkin, C. A. *Journal of the American Chemical Society* **2001**, *123*, 5164-5165.

(87) Zwanikken, J. W.; Guo, P. J.; Mirkin, C. A.; de la Cruz, M. O. *Journal of Physical Chemistry C* **2011**, *115*, 16368-16373.

(88) Alivisatos, A. P.; Johnsson, K. P.; Peng, X. G.; Wilson, T. E.; Loweth, C. J.; Bruchez, M. P.; Schultz, P. G. *Nature* **1996**, *382*, 609-611.

(89) Maye, M. M.; Nykypanchuk, D.; Cuisinier, M.; van der Lelie, D.; Gang, O. *Nature Materials* **2009**, *8*, 388-391.

(90) Xu, X. Y.; Rosi, N. L.; Wang, Y. H.; Huo, F. W.; Mirkin, C. A. *Journal of the American Chemical Society* **2006**, *128*, 9286-9287.

(91) Nykypanchuk, D.; Maye, M. M.; van der Lelie, D.; Gang, O. *Nature* **2008**, *451*, 549-552.

(92) Chen, J. I. L.; Chen, Y.; Ginger, D. S. *Journal of the American Chemical Society* **2010**, *132*, 9600-9601.

(93) Chen, J. I. L.; Durkee, H.; Traxler, B.; Ginger, D. S. *Small* **2011**, *7*, 1993-1997.

(94) Rosi, N. L.; Giljohann, D. A.; Thaxton, C. S.; Lytton-Jean, A. K. R.; Han, M. S.; Mirkin, C. A. *Science* **2006**, *312*, 1027-1030.

(95) Giljohann, D. A.; Seferos, D. S.; Daniel, W. L.; Massich, M. D.; Patel, P. C.; Mirkin, C. A. *Angewandte Chemie-International Edition* **2010**, *49*, 3280-3294.

(96) Liu, J. W.; Lu, Y. *Journal of the American Chemical Society* **2003**, *125*, 6642-6643.

Chapter II Photoswitchable Nanoparticles Assembled With Azobenzene-DNA

This chapter is mostly adapted from the original publication "Photoswitchable Oligonucleotide-Modified Gold Nanoparticles: Controlling Hybridization Stringency with Photon Dose" Yunqi Yan, Jennifer I. L. Chen, and David S. Ginger, Nano Letters, 12(5), 2530-2536, DOI: 10.1021/nl300739n

Section 2.3 is written by co-author Dr. Jennifer Chen, and modified by Yunqi Yan.

2.1 Introduction

In this chapter, I describe my studies of azobenzene-modified DNA-functionalized gold nanoparticles.[1] I show that the functionalized nanoparticles cross-link to form aggregates that can be dissociated to single nanoparticles under UV light, and that the aggregates re-form under blue light. I show that the wavelength-dependent photoisomerization enables remote optical stimuli to modulate the nanoparticle assembly process and therefore control the optical properties of the resulting solution. I further demonstrate a new and useful property of these particles: because the kinetics of the reversible photo-dissociation process depends on temperature and the relative stability of the duplex (i.e. the complementarity of the strands), light can be used to distinguish perfect from partially mismatched targets in hybridization stringency "washes" based on "photomelting".

Scheme 2.1 depicts my approach to obtain DNA-functionalized nanoparticle assemblies. I functionalized one set of 15-nm nanoparticles with 5'-thiolated azobenzene-modified DNA (Seq1Azo) and another set of 15-nm nanoparticles with a complementary native 5'-thiolated DNA (Seq2). In the initial experiment, I used a DNA sequence (Seq1Azo, see Scheme 1),

consisting of 10 natural nucleic acid bases and 4 evenly spaced azobenzenes moieties, that has been shown to photoswitch reliably in the absence of gold nanoparticles.[2]

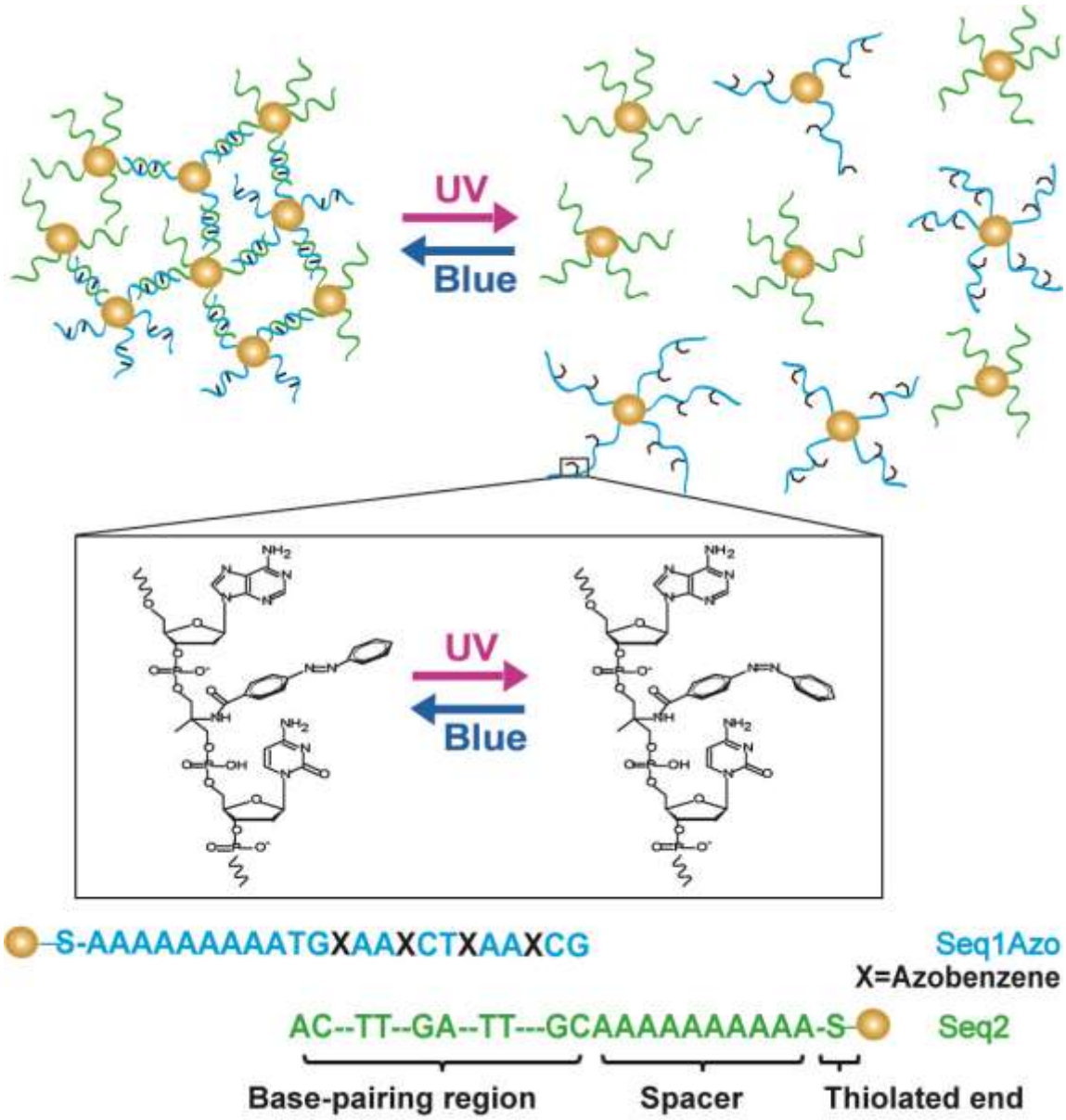

Figure 2.1 Schematic of photoswitch-modified DNA-functionalized gold nanoparticle conjugates.

Gold nanoparticles are functionalized with azobenzene-modified, thiol-terminated DNA. Hybridization of nanoparticles bearing complementary sequences is then controllable by illumination with UV and blue light via *trans-cis* photoisomerization of azobenzene.

Once prepared, the resulting DNA-functionalized gold nanoparticle (AuNP) conjugates (denoted as Seq1Azo-AuNP and Seq2-AuNP) exhibit the classic sequence-specific cross-linking typical of DNA-functionalized gold particles as seen in Figure 2.1.

2.2 Photoswitchable gold nanoparticles

Figure 2.2a shows a series of photographs demonstrating reversible optical control of DNA-directed nanoparticle assembly. Figure 2.2a(i) shows a solution of a mixture of Seq1Azo-AuNPs and Seq2-AuNPs (in 0.01 M phosphate buffer, 0.1 M NaCl and 0.01% SDS) held at room temperature for ≥ 4 h after initial mixing. The solution is nearly colorless because the DNA-linked nanoparticle aggregates have precipitated. The aggregates are visible to the naked eye as black powder on the bottom of the cuvette.

Figure 2.2a(ii) shows the same solution after being stirred under UV exposure of 0.83 mW/cm^2 (UV LED centered at 330 nm, FWHM ≤ 10nm) for 1 h at 45 ˚C (15 ˚C below gold nanoparticle assemblies' melting temperature). The solution is the bright red characteristic of dispersed gold nanoparticles (15nm in diameter) as a result of the UV-induced photomelting of the double-stranded DNA linking the aggregates together.

Exposure to blue light reverses the process, allowing the nanoparticles to reassemble into large aggregates. Figure 2.2a(iii) shows a photograph of the same solution after turning off the UV light and further exposure of the solution to 11 mW/cm^2 of blue light from the LED (wavelength centered at 470 nm, FWHM of 30 nm). After 2 h of blue irradiation under stirring and additional 20 min in the dark without stirring (to allow complete precipitation), the solution has again become colorless, with the nanoparticle aggregates visible to the naked eye as fine black powder on the bottom of the cuvette. Figure 2.2a(iv) and 2.2a(v) display images of the

same solution after one more cycle of UV and blue illumination with the same experimental treatment.

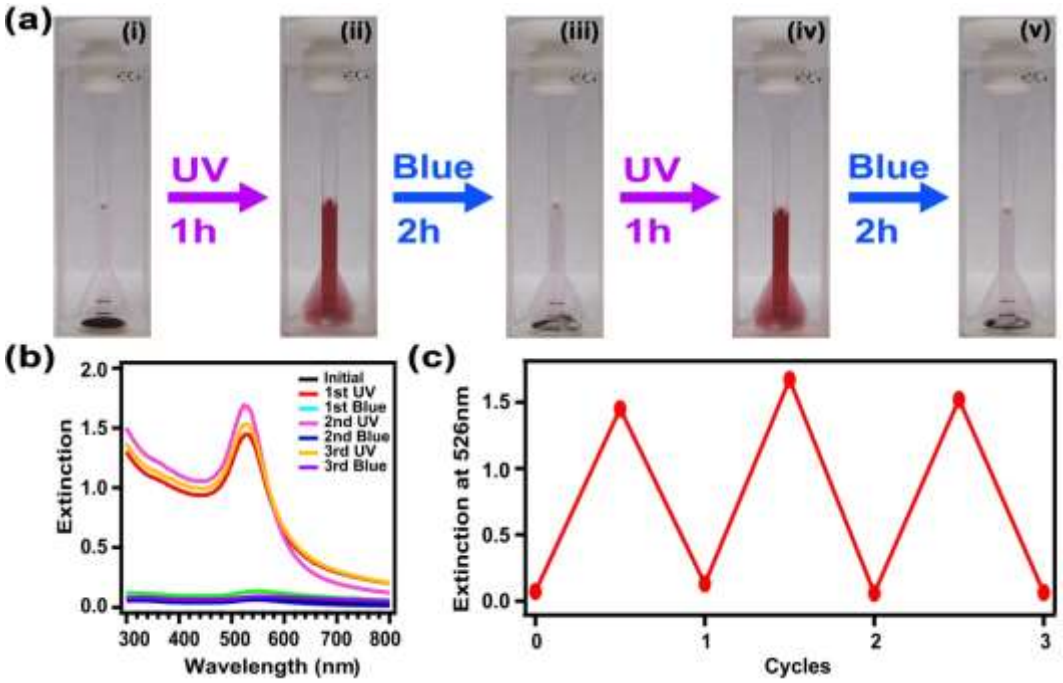

Figure 2.2 Reversible photo-controlled assembly and disassembly of DNA-nanoparticle conjugates made with azobenzene-modified oligonucleotides.

(a) Photographs of the solution containing Seq1Azo-AuNPs and Seq2-AuNPs after alternating UV and blue irradiation. (b) Corresponding UV-Vis spectra of the solution in (a) for three photoswitching cycles, with the extinction at 526 nm after each irradiation plotted in (c).

As anticipated, the photoisomerization process is reversible over many cycles. Figure 2.2b and 2.2c show the UV-vis extinction spectra and extinction changes at 526 nm, respectively, for the same solution cycled 3 times between the completely disaggregated and sedimented states. One hour of UV irradiation leads to an increase of the solution's extinction to around 1.5, with narrow LSPR at 526 nm, as large aggregates dissociate and the single gold nanoparticles become resuspended. Then, after 2 h of blue irradiation the nanoparticles again fully precipitate as large aggregates and the solution exhibits an extinction of almost zero. The negligible

variations in the extinction change after each cycle confirm that I can achieve complete and reversible photoswitching with these nanoparticles.

By studying the photoswitchable nanoparticle assemblies linked with Seq1Azo-AuNP and Seq2-AuNP, I achieved reversible photoswitching of 10 cycles with minor attenuation (Figure 2.3) by monitoring the spectroscopy features of the nanoparticle solution. The solution started as suspended nanoparticle aggregates with the typical LSPR peak at 542 nm as the starting point. I immediately irradiated the starting solution with 330-nm UV LEDs for 50 min, and I measured the LSPR of the solution blue-shifting to 526 nm. The 526-nm point corresponds to individual nanoparticle dispersion solution after the dissociation initial aggregates because of the trans-to-cis isomerization. I subsequently exposed the nanoparticle dispersion to blue LEDs for 50-60 min, and observed a red-shift LSPR peak to 542 nm, which is the peak at the starting point. In short conclusion, the 1st photoswitching cycle, monitored as LSPR peak of the solution, starts at 542 nm, changes to 526 nm after UV for 50 min, and returns back to 542 nm after blue for ~50 min. The photosiwtching cycles continues for another 9 cycles such that UV irradiation makes the peak shift to 525-526 nm for all cycles, while the blue irradiation nm leads to 542 nm only for fist 5 cycles and reduces its power to shift the peak to ~537 nm for the last 5 cycles. Azobenzene molecules are quite chemically stable under UV and blue irradiation and I noticed that longer waiting time under blue light results in larger peak shifts as larger aggregates have more time to form. I suspect that the LSPR peak attenuation might relates to the instability of DNA-linked nanoparticle system (e.g. viscosity change) that reduces the aggregation speed.

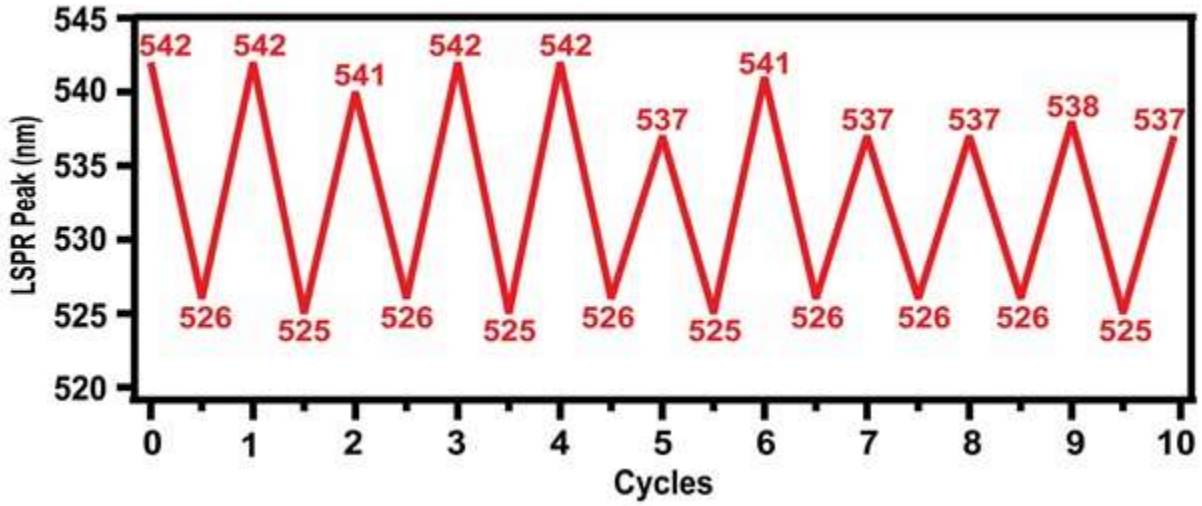

Figure 2.3 Reversible photoswitching of Seq1Azo-AuNPs and Seq2-AuNPs for 10 cycles shown by the LSPR peak shift of the solution.

For the purpose of saving time to attain more cycles, I irradiated the sample with 50 min of UV and 50–60 min of blue light. After UV irradiation, LSPR peak fully reverses to 526 nm for all 10 cycles. After blue irradiation, the peak shifts to 537 – 542 nm, corresponding to the extinction of aggregated small clusters suspended in the solution.

While gold nanoparticles can undergo local heating when illuminated,[3,4] and unusual light-induced melting has been reported,[5] I state the photomelting I describe here is due to the robust photoisomerization of the azobenzene modifications. First, the relative intensities of the UV and blue LEDs used to collect the data in Figure 2.2 are such that the blue LEDs deliver at least 10 times more absorbed power to the sample than the UV LEDs (see supporting information). Nevertheless the blue LEDs cause hybridization and aggregation, while the lower powered UV LEDs cause melting—as expected for photoisomerization-controlled melting, but inconsistent with reported photothermal and light-induced melting mechanisms.

As an additional control experiment, I irradiated the Seq1Azo-AuNPs with UV light prior to mixing them with the Seq2-AuNPs. The resulting *cis*-form Seq1Azo-AuNPs show very little aggregation with the Seq2-AuNPs, even hours after the illumination when no residual local

heating or light-induced melting could possibly be present (Figure 2.4a). In contrast, an identically prepared control mixture without any pre-mixing illumination show fast aggregation, as does a solution of Seq1Azo-AuNPs that was exposed to blue light (to photoisomerize the *cis*-azobenzene back to *trans*-azobenzene) immediately after UV exposure. Furthermore, I irradiated gold nanoparticle aggregates linked by DNA *without* azobenzene modification (Seq1 and Seq2, see supporting information for sequences) with UV and blue light as a control, and I observed no change in the extinction spectra (Figure 2.4b). This observation is in stark contrast to the spectral evolution under UV light for aggregates linked by azobenzene-modified DNA (Seq1Azo-AuNPs and Seq2-AuNPs, Figure 2.4c), where the solution extinction gradually increases and LSPR sharpens and blue shifts eventually to 526 nm, matching the spectrum of individually dispersed 15 nm-diameter gold nanoparticles.

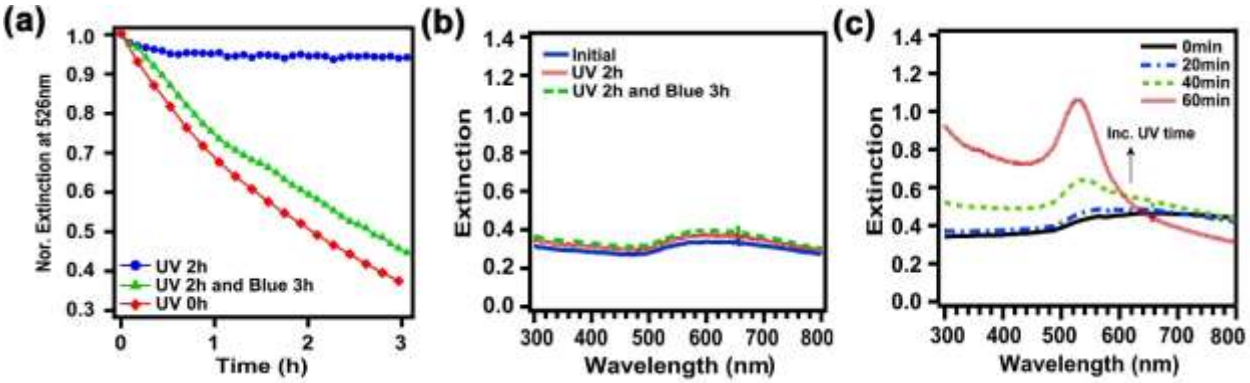

Figure 2.4 Aggregation of Seq1Azo-AuNPs and Seq2-AuNPs as monitored by UV-vis extinction at 526 nm for different pre-mixing illumination conditions on Seq1Azo-AuNPs. Illumination with UV before mixing (blue circles) prevents hybridization and nanoparticle aggregation, while nanoparticles not exposed to UV (red diamonds) or to UV then blue light (green triangles) both form aggregates. (b) Extinction spectra of control nanoparticle assemblies linked by native DNA (without azobenzene) upon UV and subsequent blue illumination. (c) Spectral evolution of Seq1Azo-AuNP and Seq2-AuNP assemblies at different UV time intervals.

I note that while azobenzene-based photocontrol of gold nanoparticle aggregation has been reported previously,[6-8] these earlier demonstrations used azobenzene that was directly covalently bonded to the gold nanoparticles using alkanethiol linkages.[9] The advantage of this approach is that it combines the opportunities of photoswitch-based control with the programmable recognition properties of DNA-functionalized nanoparticles to enable new applications. For example, aside from the obvious applications in light-controlled DNA-programmed nanoscale assembly, photoswitchable DNA-nanoparticle conjugates could be useful to discriminate specific binding from nonspecific target interference in diagnostics: because foreign or interfering species can often cause nanoparticles to precipitate from solution (resulting in false positives) in colorimetric assays, I suggest that photomelting of DNA-linked aggregates could be used as a general strategy to confirm the presence of specific targets. These photoswitchable DNA-nanoparticle conjugates also enable a unique new form of DNA-hybridization stringency as I demonstrate below.

2.3 Photoinduced disassociation of azobenzene-modified DNA-linked nanoparticle aseemblies

In order to better understand the photomelting process, Dr. Jennifer Chen initiated to investigate the temperature and photon dose dependence of the light-induced disaggregation process. I assisted her in sample preparation and instrument setup. Dr. Jennifer Chen did all measurement and data analysis. Because the relationship between the ensemble solution extinction spectrum and aggregate size is complicated by the heterogeneity and precipitation of the large aggregates, we used darkfield microscopy to measure the kinetics of photomelting on many individual, surface-attached aggregates in parallel. Figure 2.5a shows SEM calibration data confirming that the light-scattering intensity scales linearly with aggregate area. There is more

spread in our data for larger aggregates because they can be multilayer and have a wider distribution in the number of particles, but the linear correlation holds well for smaller aggregates. Hence we can derive the disaggregation kinetics by analyzing the temporal evolution of the scattered light intensity from a series of darkfield images by choosing aggregates that fall on the linear calibration curve. In a typical experiment, the sample was irradiated with continuous UV light at 375 nm, with different intensity shown in Figure 2.5b, for a total of 8–16 min with intermittent brief 106 ms exposure to darkfield light ranging from 2 to 6 s when images were captured. As the aggregates disassemble, the scattering intensity decreases with time. Typically, we analyzed 30–40 individual aggregates to obtain average disaggregation kinetics under a given set of conditions.

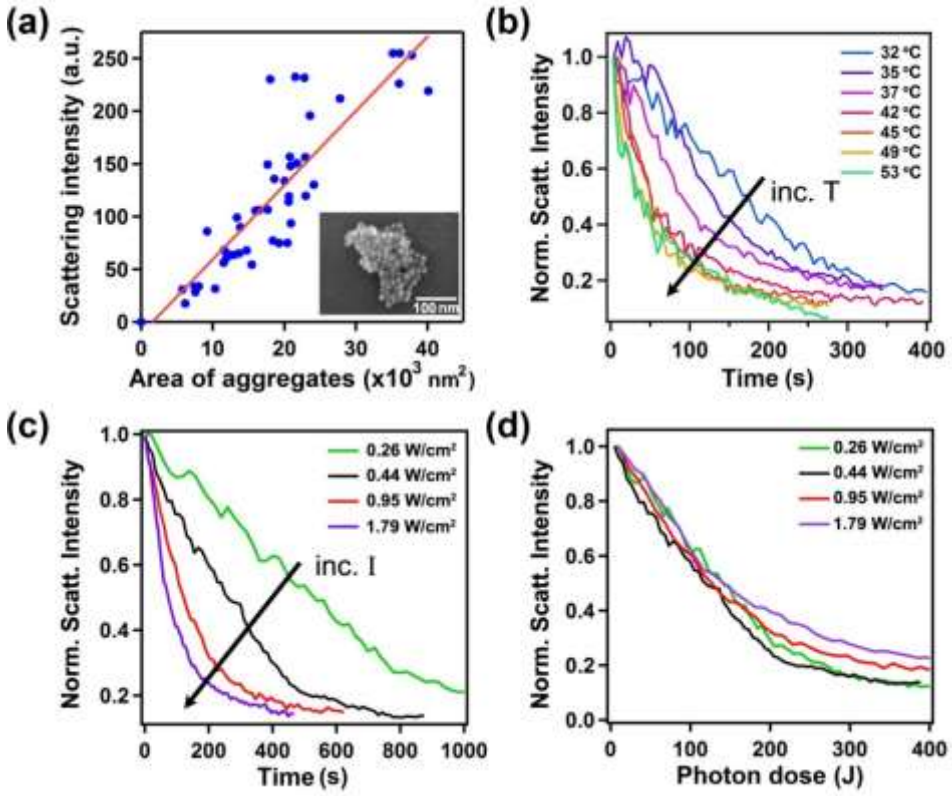

Figure 2.5 Photoinduced disaggregation kinetics of DNA-linked nanoparticle assemblies.

(a) Calibration curve showing linear dependence of scattering intensity on cross sectional area of the aggregates obtained from SEM-darkfield correlation. The linear fit is $y=-11.2\pm10.7 + 0.0070\pm0.0005x$, with a Pearson's correlation of 0.89. The inset shows a SEM image of a typical surface-anchored multi-nanoparticle assembly. Normalized scattering intensity obtained from an average of 30–40 aggregates as a function of UV irradiation time at: (b) different temperatures; and (c) different light intensities. (d) The same curves in (c) plotted as a function of photon dose.

Figure 2.5b shows the disaggregation kinetics at a series of temperatures from 32 ˚C to 53 ˚C for nanoparticle aggregates linked by Seq1Azo and Seq2. Under these conditions, the DNA-linked nanoparticle aggregates photomelt following ~6 min of exposure to UV light. It is clear that, even well below the melting temperature, the photoinduced disaggregation is temperature dependent and becomes faster at higher temperatures. We speculate that this temperature dependence may be associated with the degree of local thermal motion in the DNA helix surrounding the azobenzene photoswitches that ultimately influences the rate of photoisomerization-induced dehybridization.

Figure 2.5c shows that the light-scattering intensity of the anchored gold nanoparticle assemblies drops faster with higher UV intensity. The photomelting rate thus depends on the intensity of the UV illumination, suggesting that faster photomelting could be achieved using sufficiently intense light sources. Importantly, over the intensity ranges and temperatures investigated here, photomelting appears to be controlled by total UV photon dose. Figure 2.5d shows that the measured dissociation curves overlap when the x-axis is plotted as total photon dose, even though melting likely requires absorption of multiple photons since there are multiple azobenzenes per DNA strand, and multiple DNA strands per nanoparticle. Such photon dose dependent behavior is consistent with a negligible rate of *cis-trans* thermal isomerization over the course of the experiment. This dose-dependent behavior could be used, for example in microfluidic

and lab-on-a-chip application to minimize the need for heating, mixing and fluid processing—thus reducing system complexity.

2.4 Photo-controlled DNA hybridization stringency

I further studied this photomelting process of nanoparticles assembled by perfectly matched sequence and single-base-mismatched sequences. With the help of my advisor and Dr. Chen, we hypothesized that it would be possible to distinguish mismatched sequences from perfect sequences via controlled photon dose during photomelting to achieve a "photon stringency wash". Next, I demonstrate that photon dose stringency can indeed be used instead of conventional temperature- or salt-dependent stringency washes to distinguish single-base mismatches in target strands using these new photoswitchable DNA-functionalized nanoparticles.

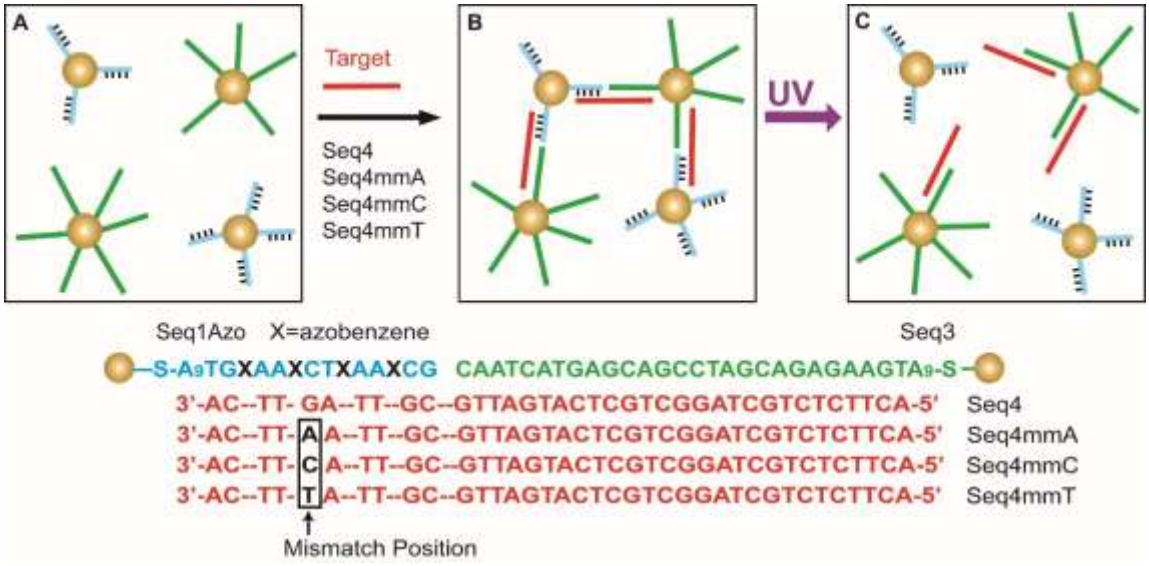

Figure 2.6 Schematic of DNA Sequences and 3-strand capture motif used in the photostringency experiments.

DNA functionalized gold nanoparticles (A) form aggregates in the presence of target nucleic acids (B), which dissociate at different rates upon UV irradiation (C) depending on the presence or absence of a single-base mismatch in the target.

For these experiments, I utilized a classic 3-strand target-probe capture strategy[10] as depicted in Figure 2.6: gold nanoparticles are functionalized with Seq1Azo and Seq3, which are each complementary to opposite ends of the target sequence (Seq4). When mixed, solutions of gold nanoparticles that are functionalized with Seq1Azo and Seq3 thus form aggregates in the presence of the Seq4 target. In addition to the perfectly complementary target, nearly complementary targets with partial sequence mismatches can also cause cross-linking of the nanoparticles.[11] Although the target linking strand is native DNA, Seq1Azo (attached to the gold nanoparticles) contains 4 azobenzenes and the resulting nanoparticle aggregates can thus be reversibly photoswitched.

Distinguishing between perfect complements and partial mismatches is an important part of DNA and RNA assays, and is usually accomplished with a stringency wash.[12] A stringency wash typically involves washing with buffers of different temperatures,[13,14] or salt concentrations,[15] with the temperature/salt concentration chosen so that the perfect complement (which is thermodynamically more stable) remains bound to the probe DNA, while the mismatched targets are preferentially dehybridized.

Figure 2.7 shows that the photoswitchable gold nanoparticles allow photon dose to be used to achieve hybridization stringency and discrimination of single base mismatches. Figure 2.7a and 2.7b show the photomelting data for four solutions of nanoparticles, one with a perfectly complementary target (Seq4) and three with single-base mismatches (Seq4mmA, Seq4mmC, Seq4mmT, see Figure 2.6) during exposure to 330 nm light from UV LEDs at 30 ˚C. I track the photomelting process by monitoring the UV-vis spectra of the solutions and plotting the LSPR peak (Figure 2.7a) and extinction change (Figure 2.7b) as a function of photon dose. Figure 2.7a shows that mismatch-linked assemblies photomelt to almost all single nanoparticles

with LSPR peaks shifting from ~560 nm to 526–528 nm. However, assemblies linked by the complementary target remain as small aggregates with a very small LSPR shift from 566 nm to 557 nm. I further examine the extinction changes at 526 nm because dispersed single gold nanoparticles in our experiment have the strongest optical response at that wavelength. Figure 2.7b shows that gold nanoparticle assemblies linked by Seq4mmC and Seq4mmA exhibit the fastest rise in extinction as they photomelt, with an overall change in extinction of ~0.5 after 1.6 J of UV light exposure. Nanoparticles linked by Seq4mmT also photomelt, though to a lesser degree over the same time period (extinction change of 0.3). On the other hand, the complementary target linked gold assemblies yield only a small increase in extinction. This trend in the photomelting kinetics is in line with the relative stability of the aggregates (i.e. the melting temperatures of assemblies are Seq4mmC ≈ Seq4mmA < Seq4mmT << Seq4, see Table 2.1).

AuNP assemblies	T_m (˚C)
Seq4	60.5
Seq4mmA	40.5
Seq4mmC	41.5
Seq4mmT	44.9

Table 2.1 Melting temperatures (T_m) of 3-strand AuNP assemblies at 0.01 M phosphate buffer, 0.05 M NaCl and 0.01% SDS.

The temperature ramp starts at 20 ˚C and ends at 60 ˚C or 80 ˚C with 1 ˚C temperature steps and 2 min hold time.

These changes in extinction can also be visualized by the color change of the solution as shown in the photographs of Figure 2.7c. Initially, after stirring and equilibration in the dark, the solutions are faintly pink as the aggregates are uniformly suspended inside the cell (did not form

sediment). After 1.6 J photon dose of UV irradiation, the color of mismatched samples transitions to red due to photomelting of the DNA-linked gold nanoparticle aggregates. In contrast, the extinction of perfect target solution hardly changes—indicating little photomelting of gold nanoparticle aggregates. These colorimetric changes demonstrate that facile discrimination of mismatches can be achieved using light, and that more detailed analysis could possibly further differentiate between the types of mismatches under certain circumstances.

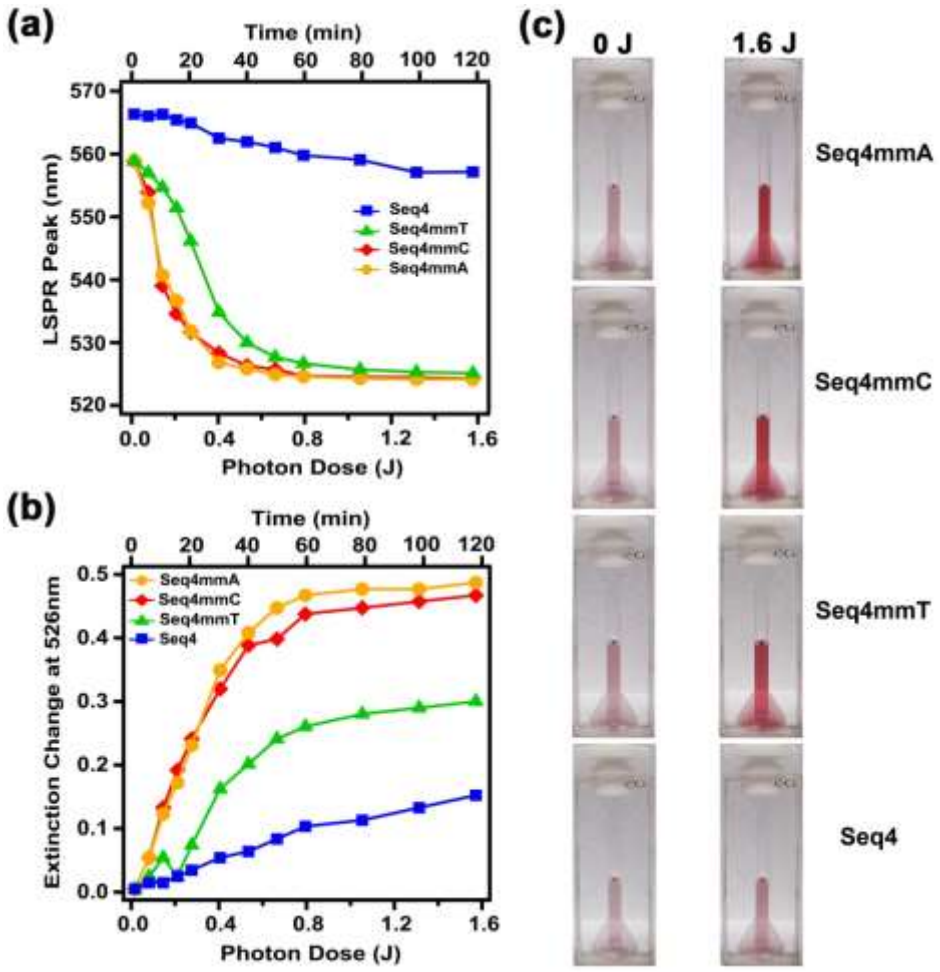

Figure 2.7. Photostringency experiments demonstrating the discrimination of complementary from single-base-mismatched sequences linking Seq1Azo-AuNP and Seq3-AuNP assemblies.

(a) LSPR peak wavelengths and (b) changes in the extinction at 526 nm of the four solutions as a function of UV photon dose. The complementary sequence (blue squares) is clearly distinguished from the single-base mismatches. (c) Photographs of the solutions before and after 1.6 J (2 h) of UV irradiation exposure.

2.5 Conclusion

In summary, I have synthesized and characterized photoswitch-modified DNA-nanoparticle conjugates. These particles exhibit new reversible stimulus-responsive properties of photoswitch-modified nanomaterials. Importantly, I have demonstrated that these materials provide a unique new means for distinguishing base-pair mismatches in DNA targets via photostringency, and offer the potential to establish new sensing platforms based on light-modulated signals.

2.6 References

(1) Yan, Y. Q.; Chen, J. I. L.; Ginger, D. S. *Nano Lett* **2012**, *12*, 2530-2536.

(2) Liang, X. G.; Mochizuki, T.; Asanuma, H. *Small* **2009**, *5*, 1761-1768.

(3) Link, S.; El-Sayed, M. A. *Int Rev Phys Chem* **2000**, *19*, 409-453.

(4) Richardson, H. H.; Carlson, M. T.; Tandler, P. J.; Hernandez, P.; Govorov, A. O. *Nano Lett* **2009**, *9*, 1139-1146.

(5) Huschka, R.; Zuloaga, J.; Knight, M. W.; Brown, L. V.; Nordlander, P.; Halas, N. J. *J Am Chem Soc* **2011**, *133*, 12247-12255.

(6) Klajn, R. *Pure Appl Chem* **2010**, *82*, 2247-2279.

(7) Klajn, R.; Wesson, P. J.; Bishop, K. J. M.; Grzybowski, B. A. *Angew Chem Int Edit* **2009**, *48*, 7035-7039.

(8) Raimondo, C.; Reinders, F.; Soydaner, U.; Mayor, M.; Samori, P. *Chem Commun* **2010**, *46*, 1147-1149.

(9) Zhang, J.; Whitesell, J. K.; Fox, M. A. *Chem Mater* **2001**, *13*, 2323-2331.

(10) Elghanian, R.; Storhoff, J. J.; Mucic, R. C.; Letsinger, R. L.; Mirkin, C. A. *Science* **1997**, *277*, 1078-1081.

(11) Taton, T. A.; Mirkin, C. A.; Letsinger, R. L. *Science* **2000**, *289*, 1757-1760.

(12) Taton, T. A.; Lu, G.; Mirkin, C. A. *J Am Chem Soc* **2001**, *123*, 5164-5165.

(13) Park, S. J.; Taton, T. A.; Mirkin, C. A. *Science* **2002**, *295*, 1503-1506.

(14) Freeman, W. M.; Robertson, D. J.; Vrana, K. E. *Biotechniques* **2000**, *29*, 1042-+.

(15) Storhoff, J. J.; Elghanian, R.; Mucic, R. C.; Mirkin, C. A.; Letsinger, R. L. *J Am Chem Soc* **1998**, *120*, 1959-1964.

Chapter III Photo-isomerization Quantum Yield Depends On DNA Sequences

This chapter is mostly adapted from the original publication "Photoisomerization Quantum Yield of Azobenzene-Modified DNA Depends on Local Sequence" Yunqi Yan, Xin Wang Jennifer I. L. Chen, and David S. Ginger, Journal of the American Chemical Society, 135(22), 8382-8387 DOI:10.1021/ja403249u

3.1 Introduction

Asanuma and co-workers have pioneered the development of an azobenzene-modified phosphoramidite,[1,2] which allows virtually any DNA sequences amenable to solid-phase synthesis to be readily functionalized with multiple azobenzene photoswitches. In this approach, the azobenzenes are incorporated by tethering them to additional sugar/phosphate linkages along the DNA backbone via a *d*-threoninol group (Figure 3.1). The incorporation of a *trans* form azobenzene stabilizes a DNA duplex by intercalation between the neighboring bases.[11] This stabilization raises the melting temperature of the azobenzene-modified DNA above that of an otherwise identical native sequence.[3] Absorption of UV light (320-370 nm) excites the $S_0 - S_2$ transition of the azobenzene groups, promoting *trans*-to-*cis* photoisomerization. In the *cis* form the azobenzenes destabilize the DNA duplex, significantly lowering the melting temperature of the DNA. Blue light (~450 nm) converts the *cis* form back to *trans*, thereby permitting reversible optical control of DNA hybridization.

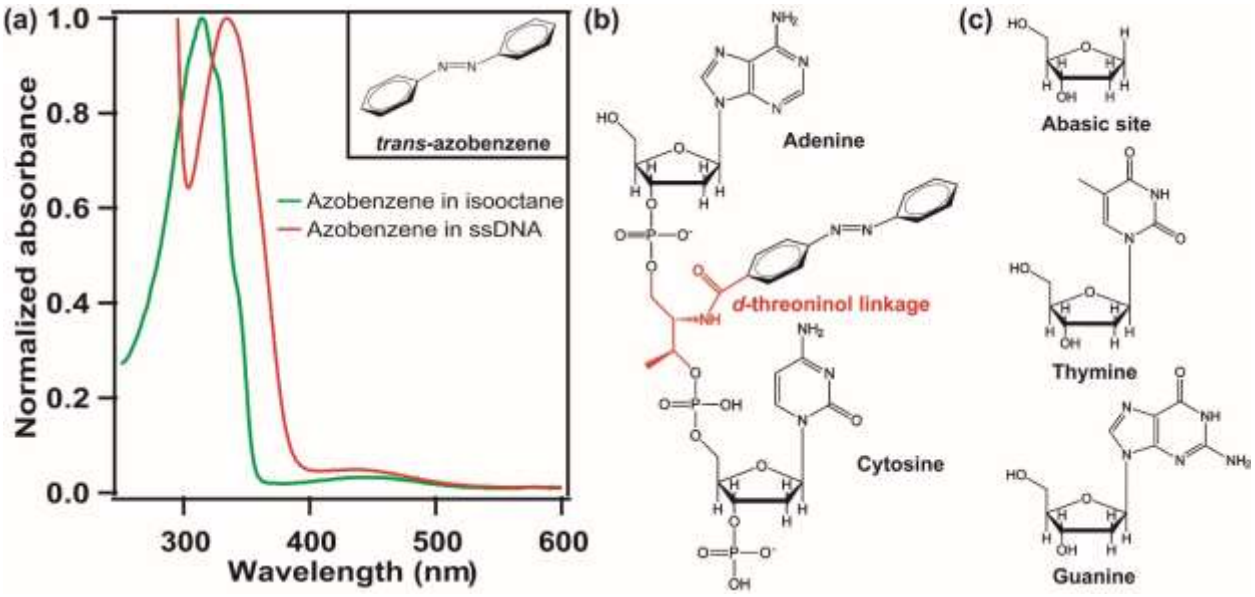

Figure 3.1 Spectra and structural features of azobenzene-modified DNA.

(a) Absorption spectra of free *trans*-azobenzene in isooctane (green) and azobenzene-modified ssDNA (red) in buffer. The structure of free azobenzene in the *trans* form is shown in the inset. (b) Structure of azobenzene-modified DNA with the *d*-threoninol linkage highlighted in red, and adenine and cytosine labeled. (c) DNA nucleotide structures of the abasic site, thymine, and guanine used in the sequences and described in the text.

These developments have enabled applications ranging from photo-controlled gene regulation,[4,5] and drug delivery,[6] to optically-powered molecular motors.[7,8] They have motivated proposals for DNA-based optical energy harvesting,[9] and even allowed the creation of DNA-hybridization assays capable of differentiating single-base mismatches using a photonic stringency wash.[10]

Virtually all of these applications are sensitive to the quantum yield for azobenzene photoisomerization: the total amount of optical energy required to achieve DNA denaturation, and the efficiency of optically-powered molecular motors will depend on the quantum yield of photoisomerization. Surprisingly, while the quantum yield for azobenzene photoisomerization is

known to depend on the local environment,[11-13] there is very little data on how the quantum yield for photoisomerization of azobenzene is affected by incorporation into different DNA sequences.

Here, I address this question by studying the quantum yield of *trans*-to-*cis* photoisomerization of azobenzenes inserted into DNA sequences via the popular Asanuma chemistry.[2] I show that the quantum yield for photoisomerization decreases upon incorporation into single stranded DNA (ssDNA), and decreases further upon incorporation into double stranded DNA (dsDNA). Importantly, I show that the quantum yield in dsDNA is sensitive to the melting temperature of the sequence and very sensitive to the presence of local mismatches.

3.2 Quantum yield decreases for azobenzene-modified DNAs

To assess how incorporation into various DNA sequences alters the *trans*-to-*cis* photoisomerization of azobenzene I measured the quantum yields in various modified DNA molecules by quantifying the fraction of *cis*-azobenzene as a function of UV (330 nm) irradiation time using UV-vis absorption spectroscopy.[11,14] Figure 3.2(a) compares the absorption spectra of free *trans*-azobenzene dissolved in isooctane and *trans*-azobenzene incorporated in ssDNA in phosphate buffer. The free azobenzene exhibits the typical π to π* absorption at 315 nm, whereas the azobenzene incorporated into ssDNA has its absorption band shifted to about 340 nm as previously reported.[15]

Figure 3.2(a) compares the fraction of *cis*-azobenzene as a function of the integrated photokinetic factor (excitation time converted to photon dose to account for the changing absorption of the solution over time) at 28 ˚C for free azobenzene, azobenzene attached via *d*-threoninol linkages to a ssDNA sequence and the same DNA sequence hybridized to its (azobenzene-free) complement. For free azobenzene, the fraction of *cis*-azobenzene at the photo-stationary state is 0.93, which decreases to 0.51 for azobenzene incorporated into ssDNA, and 0.15

for azobenzene incorporated into dsDNA. I extracted the photoisomerization quantum yield from the curves in Figure 3.2(a) by fitting the data to Equation 1:

$$y = (y_0 - y_\infty)\exp(-Ax) + y_\infty \qquad \text{Equation 1}$$

where x is the integrated photokinetic factor defined via Equation 2, y is the fraction of *cis*-azobenzene (y_0 and y_∞ are the fractions of *cis*-azobenzene before photoisomerization and at the photo-stationary state), and A is a pre-factor related to the *trans*-to-*cis* quantum yield (see supporting information for details). The integrated photokinetic factor is given by:

$$x(t) = \int_0^t \frac{1 - 10^{-abs(t)}}{abs(t)}\, dt \qquad \text{Equation 2}$$

Figure 3.2(a) shows fits of Equation 1 to the data as solid lines. From these fits I obtained a quantum yield for free azobenzene of 0.094±0.004 when excited at 330 nm, which is consistent with literature values.[14]

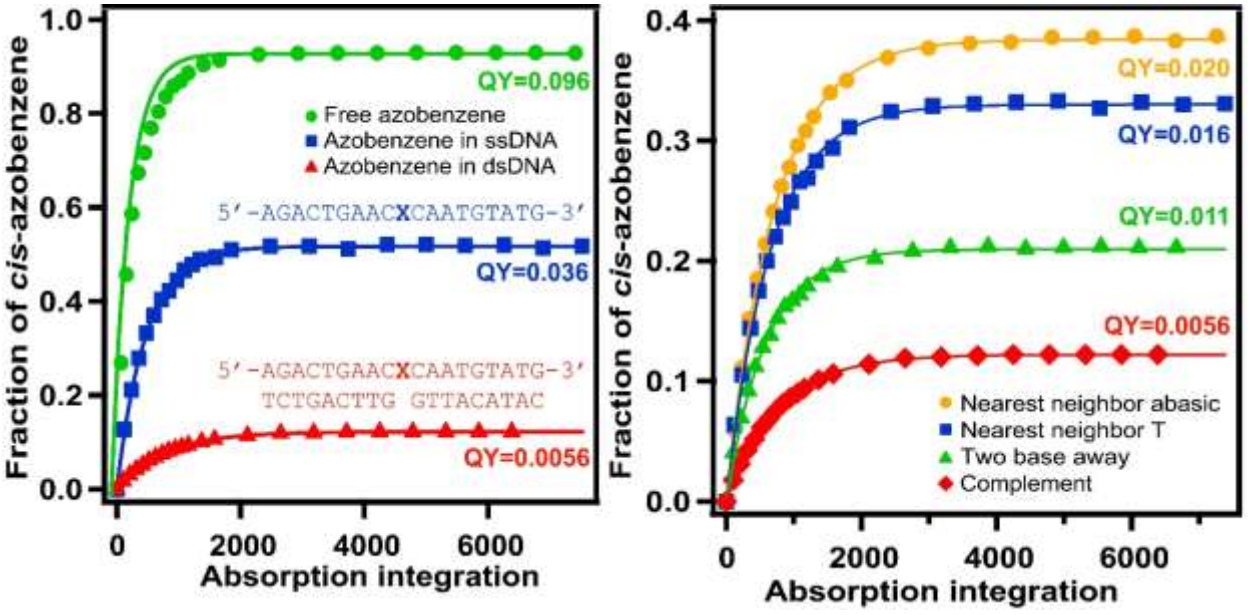

Figure 3.2 Photoinduced isomerization kinetic plots of azobenzene-modified DNA.

(a) Representative plots of the measured fraction of *cis*-azobenzene vs. the integrated photokinetic factor (Equation 2) used to obtain quantum yield. Solid lines are fits of Equation 1 to the data shown, and are labeled with the average quantum yield values measured from at least three separate experiments. Traces

are for azobenzene in isooctane (green circles), azobenzene incorporated in ssDNA (blue squares) and dsDNA (red triangles). (b) Similar plots for azobenzene incorporated in different dsDNA sequences including Seq-mm-abasic (yellow circles), Seq-mm1T (blue squares), Seq-mm2 (green triangles) and Seq-complement (red diamonds) (see Table 3.1 for sequences)

As can be seen from the decrease in *cis*-azobenzene fraction in the photo-stationary state at a given illumination intensity, incorporation into the ssDNA sequence decreases the photoisomerization quantum yield by a factor of ~3 to 0.036 ± 0.002. Hybridization of the ssDNA to its complement (Seq-complement) results in an even more dramatic decrease of the quantum yield to 0.0056 ± 0.0008. Since the DNA solutions do not absorb at the UV excitation wavelength used here, I attribute these differences entirely to the attachment of the azobenzene to the DNA sequences.

3.3 Quantum yield increases for mismatched dsDNA

While the structure—ssDNA and dsDNA—has a strong influence on the azobenzene photoisomerization quantum yield, I also find that the sequence of the dsDNA—particularly mismatches in the sequence near the azobenzene site—plays a role. To explore sequence effects, I used azobenzene-modified dsDNA with one sequence having azobenzene incorporated in the center, and the other sequence bearing a single-base mismatch at varying distance from the azobenzene site (see Table 3.1 for sequence data). Figure 3.2(b) compares the fraction of *cis*-azobenzene as a function of the integrated photokinetic factor (Equation 2) for several different dsDNA sequences at 28 ˚C. By fitting Equation 1 to the data in Figure 3.2(b), I extracted the photoisomerization quantum yields of the azobenzene in these different dsDNA sequences. The quantum yields for all studied sequences are summarized in Table 3.1. Figure 3.2(b) and the accompanying fits show that the varying fractions of *cis*-azobenzene achieved at the photo-

stationary state are due to sequence-dependent variations in the azobenzene photoisomerization quantum yield.

Of the sequences used in Figure 3.2(b), the lowest quantum yield of 0.0056 ± 0.0008 comes from azobenzene-modified dsDNA with no mismatches (Seq-complement). The quantum yield increases to 0.011 ± 0.001 for dsDNA having an A•C mismatch two bases away from the azobenzene position (Seq-mm2). In contrast, a C•T mismatch immediately next to the incorporated azobenzene (Seq-mm1T) increases the quantum yield by an additional 45% to 0.016 ± 0.001. Finally, I measure the largest quantum yield (0.020 ± 0.001) using modified dsDNA having an abasic site (with no purine or pyrimidine, Figure 3.1(c), Seq-mm-abasic) as the nearest neighbor to the azobenzene in the unmodified sequence.

Names	Sequences	Quantum Yield	T_m (˚C)
ssDNA	5′-AGACTGAAC**X**CAATGTATG-3′ **X:** azobenzene	0.036 ± 0.002	
Seq-mm-abasic (mm: mismatch)	5′-AGACTGAAC**X*C***AATGTATG-3′ TCTGACTTG ***O***TTACATAC ***O***:abasic site	0.020 ± 0.001	46.7
Seq-mm1T	5′-AGACTGAAC**X*C***AATGTATG-3′ TCTGACTTG ***T***TTACATAC	0.016 ± 0.001	48.0
Seq-mm1C	5′-AGACTGAAC**X*C***AATGTATG-3′ TCTGACTTG ***C***TTACATAC	0.015 ± 0.001	48.0
Seq-mm1A	5′-AGACTGAAC**X*C***AATGTATG-3′ TCTGACTTG ***A***TTACATAC	0.0078 ± 0.0007	48.0
Seq-mm2	5′-AGACTGAAC**X**C***A***ATGTATG-3′ TCTGACTTG G***C***TACATAC	0.011 ± 0.001	52.0
Seq-mm3	5′-AGACTGAAC**X**CA***A***TGTATG-3′ TCTGACTTG GT***G***ACATAC	0.0070 ± 0.0002	54.0
Seq-mm4	5′-AGACTGAAC**X**CAA***T***GTATG-3′ TCTGACTTG GTT***G***CATAC	0.0069 ± 0.0006	54.0
Seq-complement	5′-AGACTGAAC**X**CAATGTATG-3′ TCTGACTTG GTTACATAC	0.0056 ± 0.0008	60.0

Table 3.1 Quantum yields and melting temperatures (T_m) of the azobenzene-modified DNA.

To examine the effects of dsDNA stability and DNA sequence on quantum yield, Figure 3.3 plots the quantum yield as a function of the measured melting temperature (T_m) of the modified dsDNA sequences listed in Table 1. Broadly, the data show that the azobenzene quantum yield tends to decrease with increasing T_m of the embedding DNA sequence. I measure the highest azobenzene quantum yield (0.020±0.001) for the dsDNA with the lowest T_m (46.7˚C) (Seq-mm-abasic). Likewise, I measure the lowest photoisomerization quantum yield (0.0056±0.0008) for the dsDNA with the highest T_m (60.0˚C) (Seq-complement). Our data are consistent with previous work showing that photoisomerization can be used to modulate T_m,[12,24] but importantly, our work shows that the converse is also true: the T_m of the dsDNA sequence can in turn affect *trans*-to-*cis* isomerization efficiency.

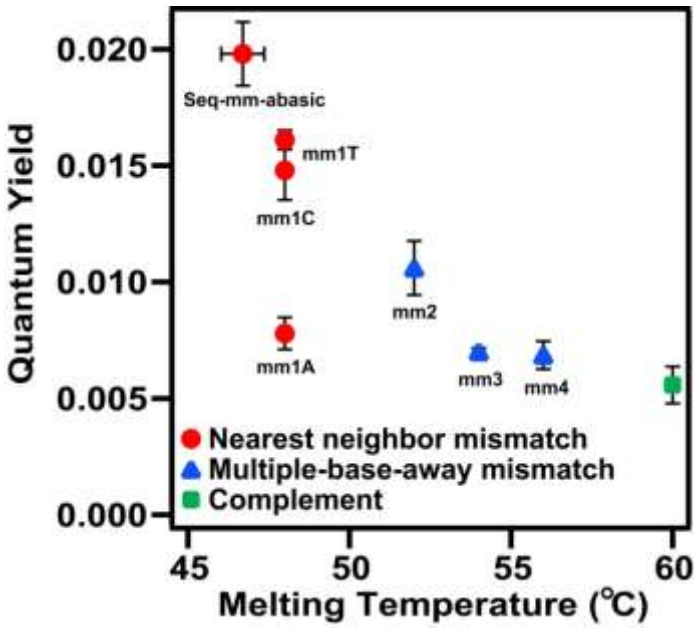

Figure 3.3 The *trans*-to-*cis* isomerization quantum yield plotted as a function of melting temperature (T_m) of azobenzene-modified dsDNA.

Quantum yield decreases as T_m rises. The quantum yield is very sensitive to the single-base mismatch at the nearest neighbor position of the azobenzene (red circles), but is less sensitive for dsDNAs having the mismatched base multiple bases away from the azobenzene (blue triangles and the green square)

Looking at these endpoints, one might be tempted to conclude that T_m is the primary controlling factor in determining the azobenzene quantum yield. However, closer inspection of the data reveals that more complicated effects are at work. For instance, Figure 3.3 shows that three sequences with very similar T_m have dramatically different quantum yields for azobenzene photoisomerization. Interestingly, all three of these sequences have a single-base mismatch immediately next to the position of the azobenzene (Seq-mm1T, Seq-mm1C, Seq-mm1A). The photoisomerization quantum yield is less sensitive to mismatches that are two or more bases away from the position of the azobenzene (e.g. Seq-mm2, Seq-mm3, Seq-mm4).

3.4 Quantum yield depends on DNA sequences

I propose that the variations I observe in photoisomerization quantum yield when the azobenzene is incorporated into DNA are largely due to differences in the local free volume available to the azobenzene in the different sequences. Generally, the azobenzene quantum yield is known to depend on the free volume surrounding the azobenzene site,[12,13] and this explanation would be consistent with our results that the quantum yield decreases on going from an azobenzene free in solution to being incorporated in ssDNA to being incorporated in dsDNA. Furthermore, this hypothesis could account for the large differences I observe between single-base mismatches that are next to the azobenzene site, and those that are further removed: distortions in the double helix are known to recover over a decay length of only a few bases.[16]

However, it is also possible that electronic interactions, including both energy and charge transfer between the azobenzene and the nucleic acid bases[17,18] are modulating the quantum yield by changing the energy relaxation pathways available to the azobenzene on an ultrafast timescale.[19] In this case, one would explain the sequence-dependent differences in quantum yield as arising from different electronic interactions between the azobenzene and the different bases.

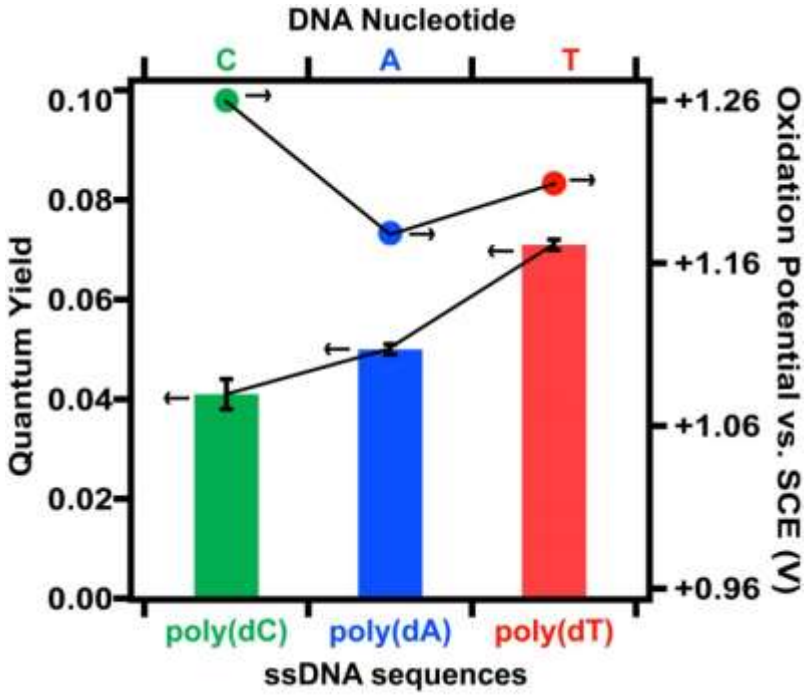

Figure 3.4 The plot of quantum yield and oxidation potential of ssDNA.

The quantum yield (bars) for the azobenzene incorporated into the 18-base ssDNA of poly(dC), poly(dA), and poly(dT). The oxidation potential for the individual DNA nucleotides (C, A, T) vs. saturated calomel electrode (SCE) is also plotted (dots). There does not appear to be a correlation between the oxidation potential for the nucleotides and the quantum yield of the azobenzene incorporated into the ssDNA sequences as might be expected if charge transfer was the dominant factor governing azobenzene quantum yield differences between the sequences.

To test this alternative hypothesis, Figure 3.4 plots the photoisomerization quantum yield (bars) for the azobenzene incorporated in the middle of 18-base ssDNAs comprising polydeoxyadenosine (poly(dA)), polydeoxycytidine (poly(dC)) and polydeoxythymidine (poly(dT)). In comparison, Figure 3.4 also plots the oxidation potential of DNA nucleotides (dots) measured in buffer (pH=7) as measured by Fukuzumi et al.[20] I note that if electronic coupling were dominant, one might expect to see some correlation between oxidation potential of the neighboring bases and the quantum yield. However, Figure 3.4 shows that the quantum yield of azobenzene contained in poly(dA), poly(dC), and poly(dT) sequences appears uncorrelated with the oxidation

potentials of the bases. On the other hand, it is known that poly(dT) is more flexible than poly(dA).[21] This result also fits well with the free volume hypothesis: azobenzene in more structurally flexible poly(dT) has a higher quantum yield than azobenzene in more rigid poly(dA).

Likewise, if energy transfer were dominant, one might expect a correlation between the positions of the UV-vis spectra of the nucleotides and the measured quantum yields – however I was unable to observe such a correlation. Figure 3.5 displays spectroscopy features of the trans-azobenzene[22] and four type of nucleotides[23] (adenosine, cytidine, guanosine, thymidine) by plotting the extinction coefficient versus wavelength at 200-500 nm. The plot clearly shows that there are no overlaps in the absorption spectroscopy for trans-azobenzene and DNA nucleotides, because trans-azobenzene shows the absorption transition around 320 m while the nucleotides show transitions well below 280 nm. Thus, I propose that free volume is likely to be more important, while acknowledging that it will be difficult to completely separate electronic and structural control over variation in the azobenzene photoisomerization quantum yield because an increase in local free volume around the azobenzene should also tend to weaken intermolecular electronic interactions.

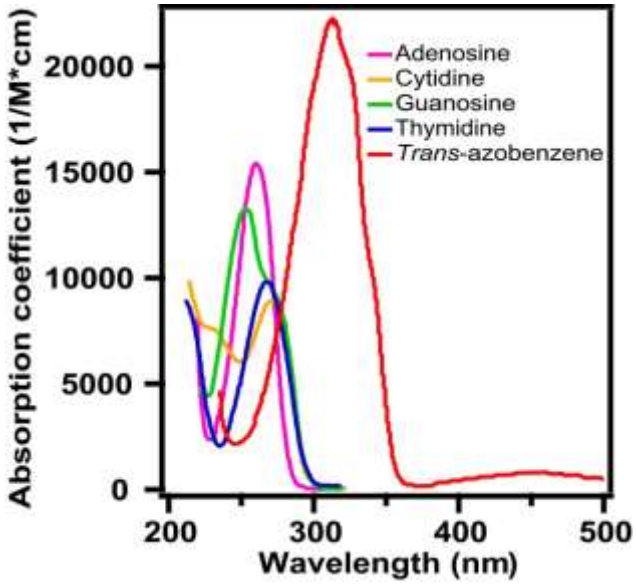

Figure 3.5 Absorption coefficient spectra of DNA nucleotides in buffer (pH=6.5) (adapted and adjusted from Handbook of Biochemistry and Molecular Biology) and *trans*-azobenzene. The spectra show that DNA nucleotides absorb photon energy mainly between 240 – 280 nm while the *trans*-azobenzene absorbs between 300 – 350 nm. There is little overlap in the transition band between DNA nucleotides and the *trans*-azobenzene.

3.5 Quantum yield of azobenzene-modified oligonucleotides explain photonic stringency

Finally, I can use the observed variation of azobenzene quantum yield with the DNA sequence to explain the properties of azobenzene-modified DNA that facilitate its use in novel DNA-hybridization assays. Previously I have shown that using only optical inputs, DNA sequences containing single-base mismatches can be resolved in hybridization experiments involving gold nanoparticles that are heavily functionalized with azobenzene-modified DNA. The resulting photonic hybridization stringency wash works because the denaturation of azobenzene-modified DNA strands occurs at lower photon doses for sequences with less complementarity. The results presented herein provide a fundamental mechanistic understanding of this process: partially mismatched sequences denature at lower photon doses because the azobenzenes in those sequences photoisomerize more efficiently than azobenzenes in perfectly complementary sequences.

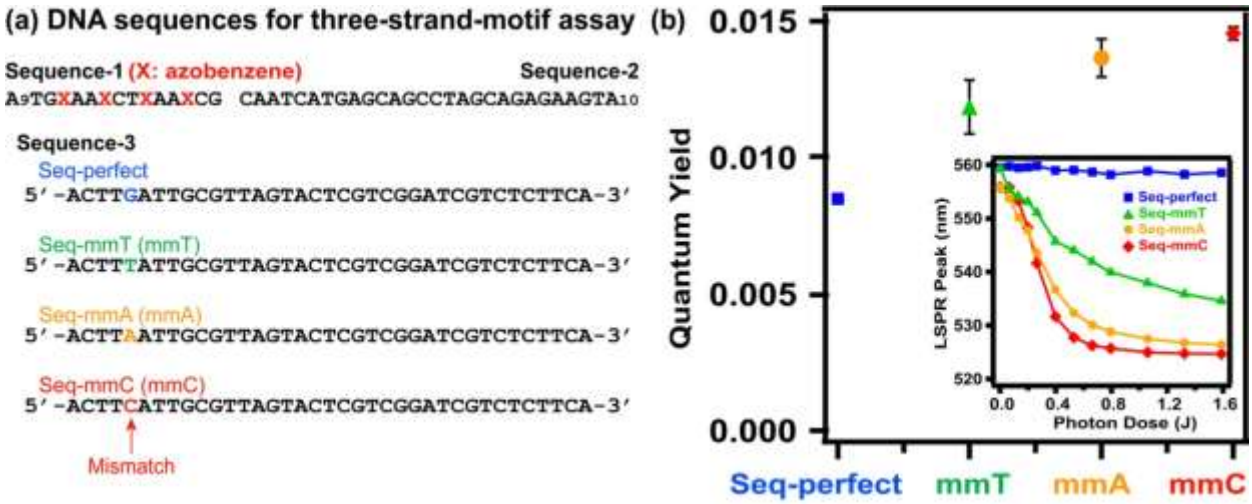

Figure 3.6 The *trans*-to-*cis* isomerization quantum yield explains photon-dose-controlled DNA hybridization stringency wash.

(a) DNA sequences used to incorporate azobenzenes and also to crosslink gold nanoparticles. (b) The quantum yield of the azobenzene is shown against each embedding dsDNA. The inset in (b) is a plot of the gold nanoparticle localized surface plasmon resonance (LSPR) peak position as a function of the photon dose. The azobenzene photoisomerization quantum yield increases from Seq-perfect, to Seq-mmT, to Seq-mmA and to Seq-mmC. Nanoparticle conjugates linked by these dsDNA show the same increasing order of photoinduced disaggregation rate.

To test this hypothesis, I measured the *trans*-to-*cis* isomerization quantum yield of azobenzenes incorporated in dsDNAs in a classic three-strand capture assay using a linker strand as shown in Figure 3.6(a). The assay consists of the capture DNA modified with multiple azobenzenes (Sequence-1), the unmodified probe DNA (Sequence-2) and the unmodified target/linker (Sequence-3) that cross-hybridizes with the capture and probe sequences. I varied the target sequence by introducing a single base mismatch in the center where it will form a mismatched base pair next to the azobenzene (See sequences in Figure 3.6(a)). I measure the lowest quantum yield for the perfectly complementary sequence (Seq-perfect), and observe an increase in quantum yield from Seq-mmA, to Seq-mmC and to Seq-mmT—all having the single-base mismatch next to one of the azobenzenes. In order to compare the trend in quantum yield

with that of optical hybridization stringency, I functionalized gold nanoparticles with the same capture and probe DNAs and measured the disaggregation rate of nanoparticle conjugates cross-linked by the same target DNA, which I have previously shown can exhibit photon-dose-controlled hybridization stringency.[5] I quantify the disaggregation rate by monitoring the localized surface plasmon resonance (LSPR) peak shift of nanoparticle conjugates, which is expected a blue shift as conjugates undergo photoinduced dissociation. Indeed, the inset in Figure 3.6(b) shows that the photon-dose dependence of the nanoparticle disaggregation process follows the exact same sequence-dependent order as the measured azobenzene quantum yields, providing strong evidence that the two trends are linked.

3.6 Control experiments exclude the influence of UV-vis illumination

Azobenzene molecules—trans-form and cis-form—absorb photonic energy at UV and visible region, which triggers the isomerization reaction. We were concerned that the UV-vis absorption spectroscopy method used to monitor the isomerization kinetics would, however, interfere the reaction because the spectrometer would illuminate the sample with wavelength at 190-1100 nm. Though the illumination intensity of the spectrometer was less than that of the excitation UV LEDs, we decided to perform the control experiment by monitoring the fraction change of azobenzene molecules that are exposed only to the UV-vis spectrometer beam.

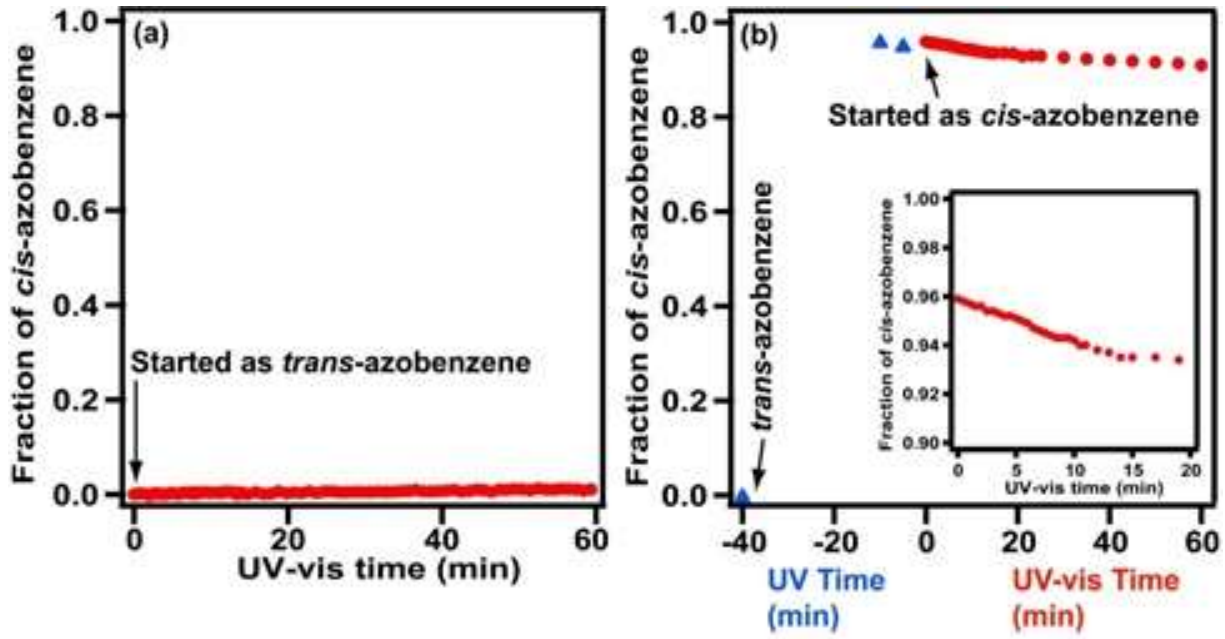

Figure 3.7 Experimental results exclude the influence of UV-vis absorption measurement on azobenzene isomerization. Fraction of *cis*-azobenzene is plotted as a function of absorption measuring time for free azobenzene in isooctane.

(a) Azobenzene started in *trans* form. The fraction of *cis*-azobenzene was almost zero after intense absorption spectrum was taken every half min for 1 h, proving that *trans*-azobenzene does not isomerize to *cis*-azobenzene after exposure to the light source of UV-vis spectrometer; (b) Azobenzene started in *cis* form after being converted from *trans* form by UV excitation. The absorption spectra were measured every 1 min for 1 h. The small decrease in the fraction of *cis*-azobenzene proves the minimal influence on *cis*-to-*trans* isomerization from UV-vis spectrometer light source.

Trans-azobenzene sample was kept in dark at room temperature with about 1-sec intermittent exposure to the spectrometer beam for 1 hr, during when there would be 40-time exposures compared to 21-time exposures for the quantum yield tests. Figure 3.7(a) plots the fraction of cis-azobenzene as function of time, the value of which started as zero and remained almost zero for the entire 40-time intermittent exposures in 1 hr. This suggests to us that the optical illumination from the spectrometer does not trigger the trans-to-cis photoisomerization reaction. Meanwhile, we did the same control experiments for the cis-azobenzene by first converting the

trans-azobenzene to the cis-form with 40-min 330-nm irradiation, which shown as "-40 min" in Figure 3.7(b). The sample, kept in dark at room temperature, started as ~ 95% of cis-azobenzene and ended as ~ 92% of cis-form after 1-hr exposure with almost 40 times of exposures. It implies to us that the cis-azobenzene slowly isomerize to the trans-form, but the rate is small enough to be neglected. Considering that cis-azobenzene can be thermally-induced to isomerize to trans-azobenzene with a half-life time being 2 days, we suspect that this slow cis-to-trans isomerization could be the thermal isomerization, which is not related to the spectrometer beam.

3.7 Conclusion

I have shown that the *trans*-to-*cis* photoisomerization quantum yield for azobenzene decreases upon incorporation into DNA, and is sensitive to both the local DNA sequence and DNA hybridization state. In general, the photoisomerization quantum yield tends to increase as the T_m of the attached dsDNA decreases. However, the biggest variations in quantum yield are associated with dsDNAs bearing a single-base mismatch immediately next to the azobenzene site. I propose that these variations arise due to the structural fluctuations caused by the adjacent mismatched base inducing an increase in the local free volume. Not only do these results provide a mechanism to explain optically-controlled DNA hybridization stringency, but I believe they will also prove useful for designing systems to more effectively photomodulate gene regulation and drug delivery, or transduce optical energy into work using DNA nano-machines.

3.8 References

(1) Asanuma, H.; Matsunaga, D.; Liu, M.; Liang, X.; Jhao, J. *Nucleic Acids Research Supplement* **2003**, 117-118.

(2) Asanuma, H.; Liang, X.; Nishioka, H.; Matsunaga, D.; Liu, M.; Komiyama, M. *Nature Protocols* **2007**, *2*, 203-212.

(3) Liang, X.; Mochizuki, T.; Asanuma, H. *Small* **2009**, *5*, 1761-1768.

(4) Yamazawa, A.; Liang, X. G.; Asanuma, H.; Komiyama, M. *Angewandte Chemie International Edition* **2000**, *39*, 2356-2357.

(5) Matsunaga, D.; Asanuma, H.; Komiyama, M. *Journal of the American Chemical Society* **2004**, *126*, 11452-11453.

(6) Kang, H.; Liu, H.; Zhang, X.; Yan, J.; Zhu, Z.; Peng, L.; Yang, H.; Kim, Y.; Tan, W. *Langmuir* **2011**, *27*, 399-408.

(7) Liang, X. G.; Tekenaka, N.; Nishioka, H.; Asanuma, H. *Nucleic Acids Symposium Series* **2008**, *52*, 697-698.

(8) Kang, H.; Liu, H.; Phillips, J. A.; Cao, Z.; Kim, Y.; Chen, Y.; Yang, Z.; Li, J.; Tan, W. *Nano Letters* **2009**, *9*, 2690-2696.

(9) McCullagh, M.; Franco, I.; Ratner, M. A.; Schatz, G. C. *Journal of the American Chemical Society* **2011**, *133*, 3452-3459.

(10) Yan, Y. Q.; Chen, J. I. L.; Ginger, D. S. *Nano Letters* **2012**, *12*, 2530-2536.

(11) Rau, H. In *Photoreactive Organic Thin Films*, Sekkat, Z.; Kroll, W., Eds.; Elsevier Incorporation, 2002, pp 3-47.

(12) Mita, I.; Horie, K.; Hirao, K. *Macromolecules* **1989**, *22*, 558-563.

(13) Victor, J. G.; Torkelson, J. M. *Macromolecules* **1987**, *20*, 2241-2250.

(14) Zimmerman, G.; Chow, L. Y.; Paik, U. J. *Journal of the American Chemical Society* **1958**, *80*, 3528-3531.

(15) Asanuma, H.; Ito, T.; Komiyama, M. *Tetrahedron Letters* **1998**, *39*, 9015-9018.

(16) McCullagh, M.; Franco, I.; Ratner, M. A.; Schatz, G. C. *Journal of Physical Chemistry Letters* **2012**, *3*, 689-693.

(17) Liang, X. G.; Asanuma, H.; Kashida, H.; Takasu, A.; Sakamoto, T.; Kawai, G.; Komiyama, M. *Journal of the American Chemical Society* **2003**, *125*, 16408-16415.

(18) Lewis, F. D.; Wu, Y. S.; Zhang, L. G.; Zuo, X. B.; Hayes, R. T.; Wasielewski, M. R. *Journal of the American Chemical Society* **2004**, *126*, 8206-8215.

(19) Chen, T.; Igarashi, K.; Nakagawa, N.; Yamane, K.; Fujii, T.; Asanuma, H.; Yamashita, M. *Journal of Photochemistry and Photobiology A: Chemistry* **2011**, *223*, 119-123.

(20) Fukuzumi, S.; Miyao, H.; Ohkubo, K.; Suenobu, T. *Journal of Physical Chemistry A* **2005**, *109*, 3285-3294.

(21) Goddard, N. L.; Bonnet, G.; Krichevsky, O.; Libchaber, A. *Physical Review Letters* **2000**, *85*, 2400-2403.

(22) Beharry, A. A.; Woolley, G. A. *Chemical Society Reviews* **2011**, *40*, 4422-4437.

(23) In *Handbook of Biochemistry and Molecular Biology*, Fasman, G., Ed.; CRC Press, 1975, p 589.

Chapter IV Photoisomerization of Azobenzene-Modified DNA on Solid Substrates

This chapter is mostly adapted with minor modifications from the manuscript "Photoinduced DNA Hybridization Stringency with Fluorescence Detection in Heterogeneous Assays " Yunqi Yan, Soumyadyuti Samai, Kristi L. Bischoff and David S. Ginger that is submitted to ACS Sensors.

4.1 Introduction

Control over the hybridization and dehybridization of DNA is essential for processes ranging from PCR[1] and gene regulation[2,3] to molecular sensing[4,5] and bio-inspired materials assembly.[6,7] In the lab, the hybridization state of DNA is usually manipulated by temperature,[8] ionic strength,[9] or the use of synthetic nucleic acids.[10,11] Recently however, the covalent incorporation of molecular photoswitches into oligonucleotides has opened up a route to control DNA hybridization using specific wavelengths of light as an external stimulus.[12-15]

By covalently linking azobenzene moieties onto the DNA backbone via the threoninol bond (Scheme 1a),[12,16] Asanuma et al have shown that light can be used to manipulate the hybridization of azobenzene-modified DNA in a reversible manner with ultraviolet light[17] due to the photoinduced isomerization of the azobenzene moieties.[18,19] Photo-control of hybridization using azobenzene-modified DNA has been demonstrated in applications such as optical regulations of gene transcription[20] and polymerase reactions,[21] and the creation of photo-reactive biomaterials,[22,23] optically-triggered drug delivery[24] and enzyme inhibition.[25] Using azobenzene-modified DNA-functionalized gold nanoparticles, I showed in chapter 2 that photon dose can be used as a variable to control hybridization stringency.[23] This effect arises from the variation of the azobenzene quantum yield with the local sequence in a way that local mismatches result in an

increase in azobenzene photoisomerization quantum yield,[26] and hence a faster decrease in DNA stability upon irradiation for partially complementary as compared to fully matched sequences.

So far, these experiments have been dominated by homogeneous solution environments. Here, motivated by the popularity of DNA chips in molecular diagnosis and genetic regulations,[27,28] I explore the possibility of using azobenzene-modified DNA on solid substrates. In chapter 4, I study photo-induced hybridization and dehybridization of azobenzene-modified DNA bound to glass substrates with fluorescently-labeled oligonucleotide targets in solution.

Scheme 1 depicts my approach. Through maleimide-thiol chemistry, azobenzene-modified capture sequences are covalently functionalized onto glass slides which are prior-treated with heterobifunctional molecules and thiol-reactive moieties. (Pease see Figure 4.1 for DNA sequences.) I detect fluorescence from immobilized azobenzene-modified DNA spots after soaking them with the hybridization solution containing rhodamine-labeled target sequences, indicating that the azobenzene-modified sequence is compatible with commercial fluorescence readout. I further study the photo-controlled dehybridization of azobenzene-modified capture sequences and fluorescent targets with slightly-different sequences under continuous 365-nm irradiation. I find that target sequences with a single-base mismatch lead to more rapid dehybridization compared to targets with matched sequences, extending the photonic hybridization stringency to azobenzene-modified DNA chips under heterogeneous environments.

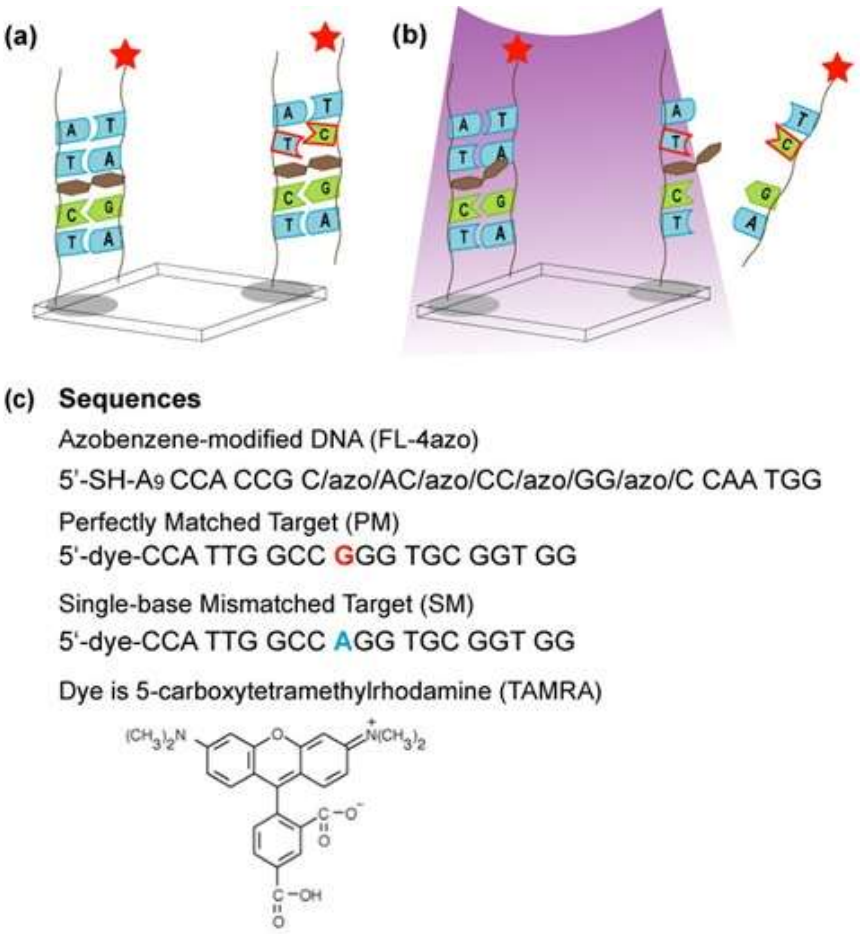

Figure 4.1 Experimental design that uses azobenzene-modified DNA microarrays.
(a) Azobenzene-modified oligonucleotides are chemically immobilized on the glass surface; target DNA (complimentary to azobenzene-modified DNA) are free of azobenzene, but are labeled with tetramethylrhodamine; target DNA binds to the surface via hybridization; cross-hybridization occurs if the target DNA varies in only one base. (b) UV light (365 nm) preferentially causes the de-hybridization of double-stranded DNA with mismatched base pairs; while perfectly matched DNA remains intact. (c) DNA sequences used in the research.

4.2 Hybridization of azobenzene-modified DNA chips

I first studied the hybridization of the functionalized azobenzene-modified capture DNA with fluorophore-labeled perfectly-matched targets. Though azobenzene has been reported to quench the fluorescence of various dye molecules,[30,31] I did not see marked quenching in this

format and was able to measure fluorescence after the hybridization. Figure 4.2(a) shows post-hybridization fluorescent images of azobenzene-modified DNA slides ("Azo" image on the right) and azobenzene-free DNA slides ("Non-azo" image on the left) with the target concentration between 0.1 nM and 1000 nM. The grey spots correspond to areas that are functionalized with DNA capture sequences. The grey scale darkness level is proportional to the emitted fluorescence intensity from target sequences that are captured by azobenzene-modified DNA. The "Non-azo" image shows control data for unmodified azobenzene-free DNA. As expected, the fluorescence intensity decreases as the target concentration reduces from 1000 nM to 10 nM. The duplicate spots on the same slide (the 2nd column in the image) show the same trend with only minor variations we attribute to variations in surface properties. Similarly, the "Azo" image—corresponding to the azobenzene-modified DNA slide—shows the expected trend of decreasing fluorescence intensity as the target concentration drops from 1000 nM to 10 nM. For both sequences, under these conditions, the fluorescence is difficult to detect when the target concentration drops to below 1 nM, consistent with literature reports.[32-34]

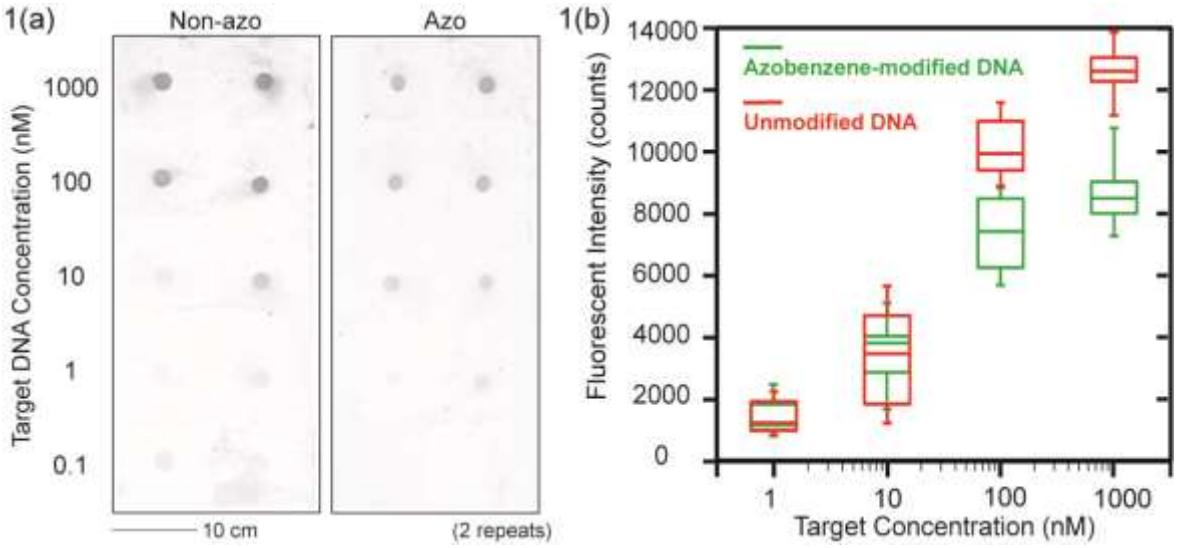

Figure 4.2. Hybridization results azobenzene-modified DNA chips.

(a) Fluorescent images of normal non-azo DNA substrates and azobenzene-modified DNA substrates after hybridization at 50 °C in 10 mM phosphate buffer. Two columns in each image are repeated data. (b) shows the box and whisker plots of fluorescent intensity counts as a function of target concentration. The box and whisker plot shows the distribution of 8-12 data points. The center line in the box is the median value; the bottom edge of the box is the 3rd quantile; the upper edge of the box is the 1st quantile; the bottom error bar is the minimum value and the upper error bar is the maximum value. The comparable fluorescent counts indicate that azobenzene-modified DNA does not quench surface fluorescence, although there is a small decrease in intensity for azobenzene-modified DNA arrays.

Figure 4.2(b) shows a box and whisker plot of the fluorescence intensity value versus the target concentration over multiple slides, reflecting the distribution of slide-to-slide variability associated with our manual spotting. The center line of the box is the median value; the bottom edge of the box is the 3rd quantile; the upper edge of the box is the 1st quantile; the bottom error bar is the minimum value and the upper error bar is the maximum value. Both the slides with azobenzene-modified capture sequences, and the azobenzene-free control slides show the expected increase in fluorescence intensity with DNA concentration. Importantly, despite reports of azobenzene being able to quench the emission of nearby fluorophores via pi-pi interactions,[30,31] the signal from the fluorescent DNA captured onto the azobenzene-modified spots was almost as intense as that captured on the control slides, with only a small (25% - 32%) decrease in the fluorescence median value for the azobenzene-modified slides being observed at the highest target concentrations. I thus thus conclude that DNA chips functionalized with azobenzene-modified capture sequences are compatible with commercial fluorescent readout.

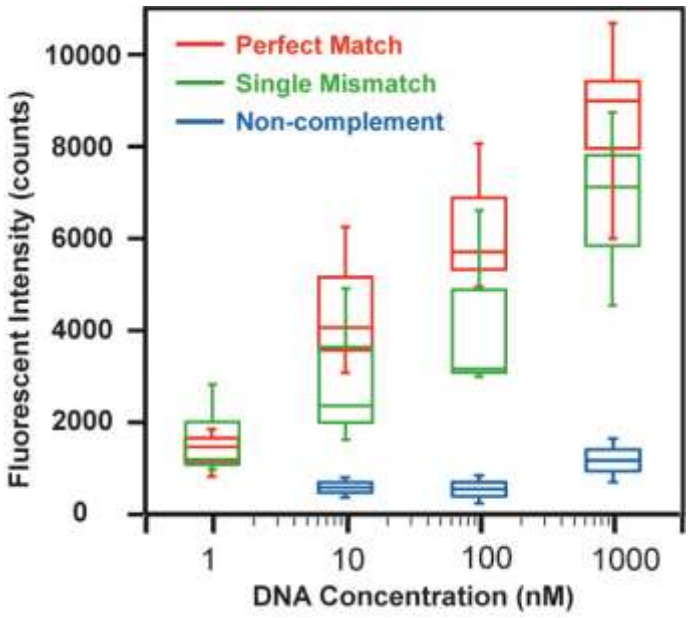

Figure 4.3 Hybridization results of perfectly-matched targets, single-base-mismatched targets, and non-complementary DNAs using azobenzene-modified DNA substrates.
Using azobenzene-modified DNA substrates, we compared the hybridization of perfectly-matched targets, single-base-mismatched targets, and non-complementary DNA. The non-complementary DNA (the control sample) shows very low fluorescence intensity after hybridization, indicating only a small degree of non-specific binding. In addition, the average fluorescence intensity is plotted as a function of target DNA concentration. Perfect matches exhibit higher fluorescence intensity than those of single mismatches from 10 nM to 1 μM.

Next, I compared the fluorescence signal under low stringency conditions (10 mM phosphate buffer, 0.01M NaCl, and temperature is 50°C) for three different sequences captured onto azobenzene-functionalized slides. Figure 4.3 shows a box and whisker plot of fluorescence intensity versus target concentration for azobenzene-functionalized slides with the perfectly-matched target (red circles), the single-base-mismatched target (green triangles) and the non-complementary target (blue diamonds). As expected, both the perfectly-matched and single-base-mismatched targets bind under these conditions and show increasing fluorescence intensity with increasing target DNA concentration. Consistent with its slightly lower binding affinity, the

median fluorescence intensity from the partially-mismatched sequence is slightly lower than the fluorescence signal from the perfect complement. As expected, the non-complementary control sequences shows much lower binding and almost no change in fluorescence up to concentrations of 1000 nM, and allowing us to estimate the background level due to non-specific binding.

In addition to the aforementioned maleimide-epoxy chemistry, I studied the amine-epoxy attachment chemistry using azobenzene-modified capture sequences with amine functionality and same target sequences labeled with tetramethylrhodamine. (See Chapter 5.10 for attachment chemistry). Figure 4.4 shows the hybridization results of azobenzene-functionalized slides with perfectly-matched (red), single-base-mismatched (green), and non-complementary targets (blue) by plotting fluorescence intensity as a function of target concentration. As expected, hybridization with completely-complementary and partially-complementary sequences show detectable fluorescence intensities that are 5 – 8 times higher than intensities of non-complementary targets across all concentrations studied here. I thus conclude that azobenzene-modified DNA arrays, regardless of surface attachment chemistry, are compatible with surface fluorescence readout upon hybridization with complementary fluorophore-labeled targets.

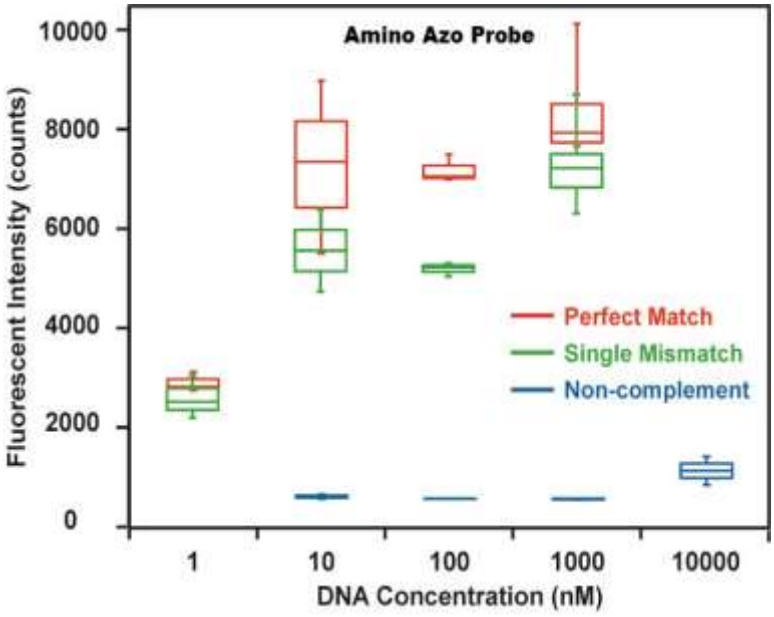

Figure 4.4 The graph of fluorescent intensity in counts versus target concentration in nM for amino-functionalized azo-DNA chips.

It shows that the amino azobenzene-modified capture sequences can hybridize to the perfectly matched targets (red circles) and single-base mismatched targets (green triagles), however, the probes cannot hybridize to non-complement sequences (blue diamonds). The plot implies that azobenzene-modified DNA chips, regardless of thiol-maleimide attachment or amino-epoxy chemistry, are compatible with the fluorescent detection method.

4.3 Photoinduced dehybridization of azobenzene-modified chips

Next, I study photoinduced dehybridization of the DNA upon exposure to UV light, made possible by incorporation of the azobenzene modifications into the capture strands. Figure 4.5(a) shows fluorescent images of azobenzene-functionalized slides before/after UV irradiation (365 nm, 6.99±0.05 mW/cm^2, 30 min), tested for both complementary targets and single-base-mismatched targets. The spots capturing target DNA are dark with intense fluorescence prior to UV exposure. The spots fade as 365-nm photons induce azobenzene photoisomerization and thus dehybridization of captured targets. Importantly, the intensity of the single-base-mismatched DNA spot decreases more (becomes fainter) than that of the perfectly-matched DNA. Figure 4.5(b) shows the corresponding data of fluorescence intensity changes for a number of samples in a box and whisker format. The median value of the fluorescence intensity of single-base-mismatched targets reduces by ~76% while the median of perfectly-matched targets drops by a lesser extent after UV.

One might worry that exposure of the fluorescently-labeled DNA to UV light could result in premature photobleaching. However, any photobleaching is much smaller than changes due to photoinduced dehybridization. Figure 3(c) and 3(d) show control experiments using azobenzene-free DNA chips and demonstrate much smaller losses in intensity (~5-10%) under same UV illumination conditions. Compared to the significant reduction observed on azobenzene-

functionalized slides, we conclude that the decrease in fluorescence intensity is due to the light-induced dehybridization of the azobenzene-modified capture sequences.

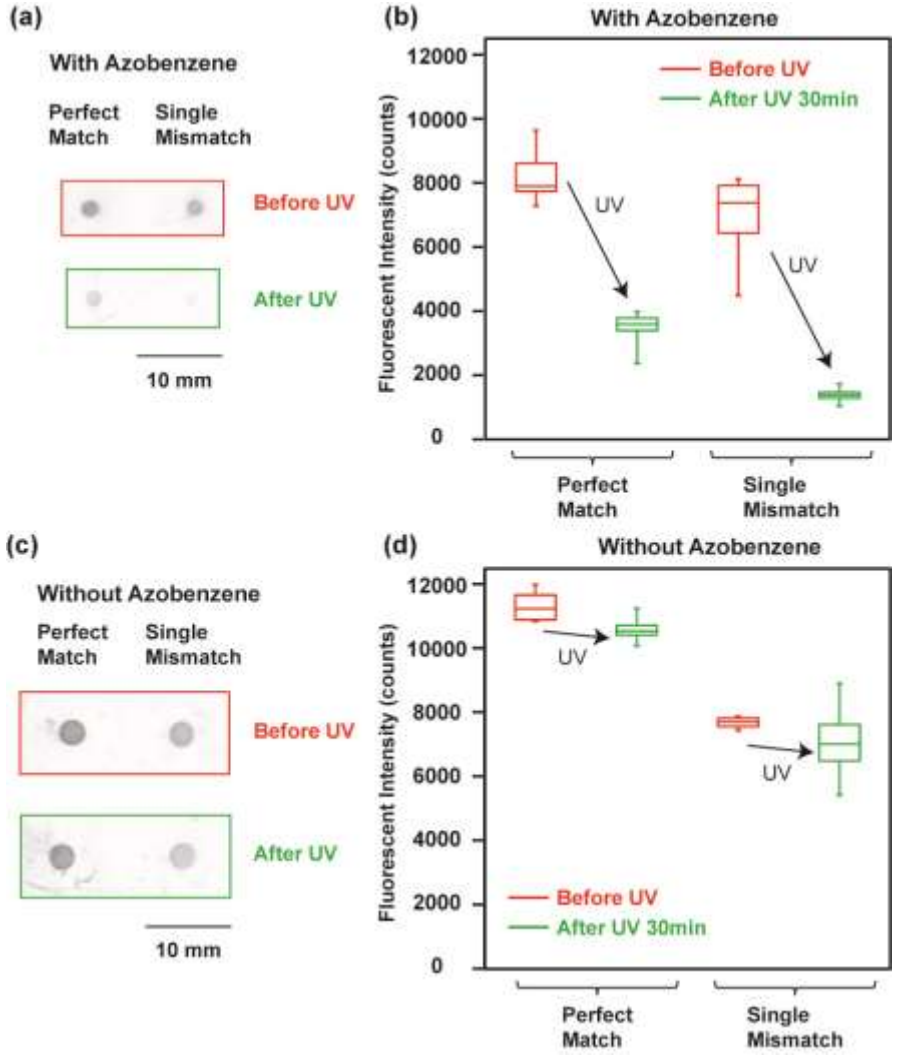

Figure 4.5 Photo-induced DNA de-hybridization happens at solid-liquid interface only on azobenzene-modified DNA arrays.

Fluorescent images are shown for azobenzene-modified DNA chips (a) and azobenzene-free DNA chips (b) before and after UV irradiation in which both perfectly-matched targets and partially-matched targets are studied. The corresponding box and whisker plots are shown in (c) for azobenzene-modified slides and in (d) for azobenzene-free slides. The fluorescence intensity decreases for azobenzene-modified slides after the irradiation while the fluorescence barely changes for azobenzene-free slides, indicating that the photoinduced dehybridization happening on the surface is due to the photoisomerization of azobenzene-modified DNA.

4.4 Photonic hybridization stringency with azobenzene-modified DNA chips

Next, I explore the possibility of photon dose to control hybridization stringency for DNA bound to solid surfaces. Figure 4.6 shows the plot fluorescence intensity as a function of UV irradiation time in a box and whisker format for target DNA with perfectly-matched sequences and single-base-mismatched sequences. Initially, the ratio of fluorescence intensities between the perfectly complementary and partially mismatched sequences is only ~1:1. After only 60 seconds of UV exposure, the fluorescence from the spot with the single-base mismatch has decreased by ~50%, while the intensity of the spot with the perfect complement has dropped by only ~7%, making the ratio of intensities increase to ~2:1 (complement: mismatch). At longer times (higher doses) the perfect complement also begins to show more significant dehybridization (decreasing to ~50% of its initial intensity after 5 min) but the partially mismatch sequence also continues to drop, and the ratio of intensities continues to increase to ~3:1 (complement: mismatch). After 10 minutes at this intensity the ratio begins to plateau around ~3:1 (complement:mismatch) under these conditions. We attribute the more rapid decrease in fluorescence observed with the single-base mismatches due to the more rapid dehybridization of mismatched sequences under UV. This result is consistent with the sequence-dependent quantum yield for azobenzene photoisomerization that we have previously measured.[37] We anticipate that this rapid change in differential hybridization (~1-5 min) achieved with the use of a low-cost commercial UV LED and without change in temperature or buffer conditions will be of interest as a possible new way to control hybridization stringency with external stimulus in DNA assays.

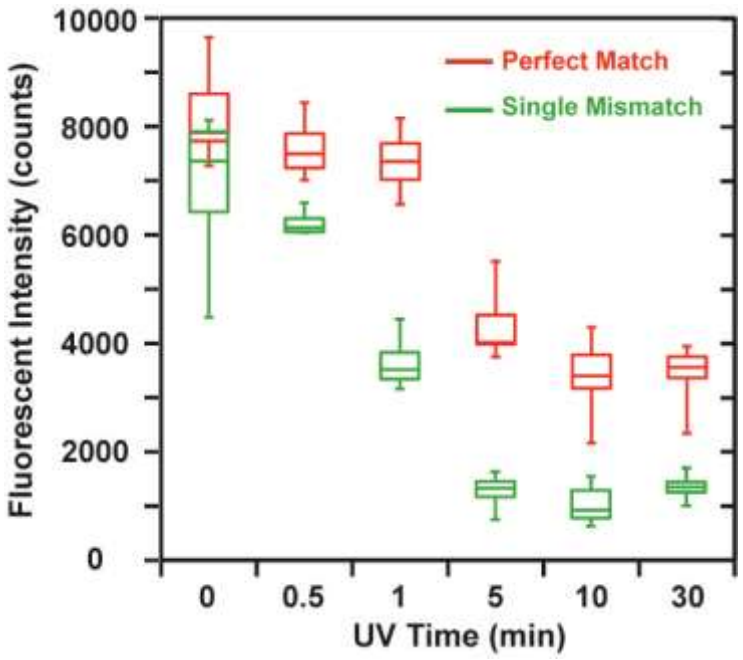

Figure 4.6 Photo-induced differential de-hybridization between perfectly-matched and single-base-mismatched targets.

I observe photo-induced differential de-hybridization between perfectly-matched and single-base-mismatched targets. I plotted the fluorescent intensity versus UV time (UV at 365 nm, 6.94±0.04 mW/cm^2). At UV 30 seconds, I measured little decrease in fluorescence for both types of targets. However, in 1 minute I began observing decrease in fluorescence between perfectly-matched sequences (~10% decrease) and sequences with a single-base mismatch (~40% decrease). I observe larger decrease in fluorescence for single-base-mismatched target when UV irradiates longer than 1 minute. At equilibrium, single-base-mismatched targets exhibit ~80% decrease in fluorescence while perfectly-matched targets exhibit ~60% decrease.

4.5 Conclusion

I have demonstrated that azobenzene-modified DNA immobilized on solid chips as capture sequences is compatible with fluorescence readout using a commercial array scanner. Furthermore, I show that I can photoswitch azobenzene molecules on a surface in the presence of fluorophores, and that I can use light to control the dehybridization behavior of the azobenzene-modified DNA immobilized on surface with the target sequences in solution. Most importantly, I

demonstrate the successful use of azobenzene-modified DNA as a means to achieve photonic hybridization stringency on heterogeneous assays with the ability to distinguish sequences with single-base resolution.

4.6 References

(1) Takei, F.; Nakatani, K. The Chemistry of PCR Primers: Concept and Application.*Isr. J. Chem.* **2013**, *53*, 401-416.

(2) Townsend, J. P.; Taylor, J. W. In *Molecular Evolution: Producing the Biochemical Data, Part B*; Zimmer, E. A., Roalson, E. H., Eds. 2005; Vol. 395, p 597-+.

(3) Aharonowitz, Y.; Cohen, G.; Martin, J. F. PENICILLIN AND CEPHALOSPORIN BIOSYNTHETIC GENES - STRUCTURE, ORGANIZATION, REGULATION, AND EVOLUTION.*Annual Review of Microbiology* **1992**, *46*, 461-495.

(4) Chen, J. I. L.; Chen, Y.; Ginger, D. S. Plasmonic Nanoparticle Dimers for Optical Sensing of DNA in Complex Media.*J. Am. Chem. Soc.* **2010**, *132*, 9600-9601.

(5) Blum, A. P.; Kammeyer, J. K.; Rush, A. M.; Callmann, C. E.; Hahn, M. E.; Gianneschi, N. C. Stimuli-Responsive Nanomaterials for Biomedical Applications.*J. Am. Chem. Soc.* **2015**, *137*, 2140-2154.

(6) Zhang, X. N.; Wang, R.; Xue, G. Programming macro-materials from DNA-directed self-assembly.*Soft Matter* **2015**, *11*, 1862-1870.

(7) Park, S. J.; Lazarides, A. A.; Mirkin, C. A.; Letsinger, R. L. Directed assembly of periodic materials from protein and oligonucleotide-modified nanoparticle building blocks.*Angewandte Chemie-International Edition* **2001**, *40*, 2909-2912.

(8) Taton, T. A.; Lu, G.; Mirkin, C. A. Two-color labeling of oligonucleotide arrays via size-selective scattering of nanoparticle probes.*J. Am. Chem. Soc.* **2001**, *123*, 5164-5165.

(9) Park, S. J.; Taton, T. A.; Mirkin, C. A. Array-based electrical detection of DNA with nanoparticle probes.*Science* **2002**, *295*, 1503-1506.

(10) Noerholm, M.; Bruus, H.; Jakobsen, M. H.; Telleman, P.; Ramsing, N. B. Polymer microfluidic chip for online monitoring of microarray hybridizations.*Lab Chip* **2004**, *4*, 28-37.

(11) Singh, R. P.; Oh, B. K.; Choi, J. W. Application of peptide nucleic acid towards development of nanobiosensor arrays.*Bioelectrochemistry* **2010**, *79*, 153-161.

(12) Asanuma, H.; Liang, X.; Nishioka, H.; Matsunaga, D.; Liu, M.; Komiyama, M. Synthesis of azobenzene-tethered DNA for reversible photo-regulation of DNA functions: hybridization and transcription.*Nat. Protoc.* **2007**, *2*, 203-212.

(13) Liang, X. G.; Asanuma, H.; Kashida, H.; Takasu, A.; Sakamoto, T.; Kawai, G.; Komiyama, M. NMR study on the photoresponsive DNA tethering an azobenzene. Assignment of the absolute configuration of two diastereomers and structure determination of their duplexes in the trans-form.*J. Am. Chem. Soc.* **2003**, *125*, 16408-16415.

(14) McCullagh, M.; Franco, I.; Ratner, M. A.; Schatz, G. C. DNA-Based Optomechanical Molecular Motor.*J. Am. Chem. Soc.* **2011**, *133*, 3452-3459.

(15) Sengupta, E.; Yan, Y. Q.; Wang, X.; Munechika, K.; Ginger, D. S. Dynamic Force Spectroscopy of Photoswitch-Modified DNA.*Acs Nano* **2014**, *8*, 2625-2631.

(16) Asanuma, H.; Ito, T.; Komiyama, M. Photo-responsive oligonucleotides carrying azobenzene in the side-chains.*Tetrahedron Lett.* **1998**, *39*, 9015-9018.

(17) Liang, X.; Mochizuki, T.; Asanuma, H. A Supra-photoswitch Involving Sandwiched DNA Base Pairs and Azobenzenes for Light-Driven Nanostructures and Nanodevices.*Small* **2009**, *5*, 1761-1768.

(18) Rau, H. In *Photoreactive Organic Thin Films*; 1st ed.; Sekkat, Z., Kroll, W., Eds.; Elsevier Incorporation: 2002, p 3-47.

(19) Bandara, H. M. D.; Burdette, S. C. Photoisomerization in different classes of azobenzene.*Chem. Soc. Rev.* **2012**, *41*, 1809-1825.

(20) Liu, M. Z.; Asanuma, H.; Komiyama, M. Azobenzene-tethered T7 promoter for efficient photoregulation of transcription.*J. Am. Chem. Soc.* **2006**, *128*, 1009-1015.

(21) Yamazawa, A.; Liang, X. G.; Asanuma, H.; Komiyama, M. Photoregulation of the DNA polymerase reaction by oligonucleotides bearing an azobenzene.*Angew. Chem. Int. Ed.* **2000**, *39*, 2356-2357.

(22) You, M. X.; Huang, F. J.; Chen, Z.; Wang, R. W.; Tan, W. H. Building a Nanostructure with Reversible Motions Using Photonic Energy.*Acs Nano* **2012**, *6*, 7935-7941.

(23) Yan, Y. Q.; Chen, J. I. L.; Ginger, D. S. Photoswitchable Oligonucleotide-Modified Gold Nanoparticles: Controlling Hybridization Stringency with Photon Dose.*Nano Lett.* **2012**, *12*, 2530-2536.

(24) Yuan, Q.; Zhang, Y. F.; Chen, T.; Lu, D. Q.; Zhao, Z. L.; Zhang, X. B.; Li, Z. X.; Yan, C. H.; Tan, W. H. Photon-Manipulated Drug Release from a Mesoporous Nanocontainer Controlled by Azobenzene-Modified Nucleic Acid.*Acs Nano* **2012**, *6*, 6337-6344.

(25) Kim, Y. M.; Phillips, J. A.; Liu, H. P.; Kang, H. Z.; Tan, W. H. Using photons to manipulate enzyme inhibition by an azobenzene-modified nucleic acid probe.*Proc. Natl. Acad. Sci. USA* **2009**, *106*, 6489-6494.

(26) Yan, Y. Q.; Wang, X.; Chen, J. I. L.; Ginger, D. S. Photoisomerization Quantum Yield of Azobenzene-Modified DNA Depends on Local Sequence.*J. Am. Chem. Soc.* **2013**, *135*, 8382-8387.

(27) Fritzsche, W.; Taton, T. A. Metal nanoparticles as labels for heterogeneous, chip-based DNA detection.*Nanotechnology* **2003**, *14*, R63-R73.

(28) Hacia, J. G. Resequencing and mutational analysis using oligonucleotide microarrays.*Nature Genetics* **1999**, *21*, 42-47.

(29) Chrisey, L. A.; Lee, G. U.; OFerrall, C. E. Covalent attachment of synthetic DNA to self-assembled monolayer films.*Nucleic Acids Res.* **1996**, *24*, 3031-3039.

(30) Grimes, A. F.; Call, S. E.; Vicente, D. A.; English, D. S.; Harbron, E. J. Toward efficient photomodulation of conjugated polymer emission: Optimizing differential energy transfer in azobenzene-substituted PPV derivatives.*J. Phys. Chem. B* **2006**, *110*, 19183-19190.

(31) Isoshima, T.; Ito, E.; Ubukata, T.; Hara, M. Fluorescence dynamics of organic laser dyes in azobenzene polymer.*Molecular crystals and liquid crystals* **2006**, *444*, 81-86.

(32) Vaidya, A. A.; Norton, M. L. DNA attachment chemistry at the flexible silicone elastomer surface: Toward disposable microarrays.*Langmuir* **2004**, *20*, 11100-11107.

(33) Rao, A. N.; Rodesch, C. K.; Grainger, D. W. Real-Time Fluorescent Image Analysis of DNA Spot Hybridization Kinetics To Assess Microarray Spot Heterogeneity.*Anal. Chem.* **2012**, *84*, 9379-9387.

(34) Broderick, A. H.; Carter, M. C. D.; Lockett, M. R.; Smith, L. M.; Lynn, D. M. Fabrication of Oligonucleotide and Protein Arrays on Rigid and Flexible Substrates Coated with Reactive Polymer Multilayers.*Acs Applied Materials & Interfaces* **2013**, *5*, 351-359.

Chapter V Experimental Methods

5.1 Surface-functionalization of gold nanoparticles with azobenzene-modified DNA

Colloidal gold nanoparticles (AuNPs) of 15 nm in diameter (~10^{12} particles/mL) were purchased from Ted Pella Inc. and used as received. All oligonucleotides were purchased from Integrated DNA Technology. Water used was deionized to 18.2 MOhm with Millipore filtration system.

Aliquots of thiolated DNA sequences (Seq1Azo, Seq1, Seq2, Seq3) were freshly cleaved by incubating with 0.1 M DTT (dithiothreitol, 0.17 M phosphate, pH=8.0) for 15 min and subsequently purified with a Bio-Spin Column. The resulting volume of 30-40 μL of DNA in water (O.D. = ~2.0 at 260 nm) was combined with 900 μL of 15 nm AuNP solution. The mixture was vortexed and sonicated, and left for 20 min at room temperature. The solution was then brought to 0.01% SDS using 1% SDS stock and 0.01 M PBS (Phosphate buffered saline, 0.137 M NaCl) using 0.1 M PBS stock. In the subsequent steps, the NaCl concentration was gradually raised to 0.4 M in increments of 0.05-0.1 M by adding buffer solution of 2 M NaCl, 0.01 M PBS and 0.01% SDS while keeping the concentration of PBS and SDS constant.[1] After each addition of NaCl, the solution was sonicated for 1 min and then incubated for 20 minutes (at room temperature for most sequences, 45 ^{o}C for Seq1Azo-AuNP) and finally incubated overnight at 0.4 M NaCl at room temperature. The DNA-functionalized AuNP (DNA-AuNP) samples were washed 3 times by repeated centrifugation and redispersion into 400 μL 0.01% SDS solution, and eventually diluted back to 900 μL of 0.01 M phosphate buffer (pH=6.6), 0.1 M NaCl, 0.01% SDS and 0.02% sodium azide for storage at 4˚C in the dark.

DNA sequences:

Seq1Azo. 5’-S-AAAAAAAAATGXAAXCTXAAXCG-3’, X = Azobenzene

Seq1. 5’-S-AAAAAAAAATGAACTAACG-3’

Seq2. 5’-S-AAAAAAAAAACGTTAGTTCA-3’

Seq3. 5’-CAATCATGAGCAGCCTAGCAGAGAAGTAAAAAAAAAA-S-3’

Seq4. 5’-ACTTCTCTGCTAGGCTGCTCATGATTGCGTTAGTTCA-3’

Seq4mmA. 5’-ACTTCTCTGCTAGGCTGCTCATGATTGCGTTAATTCA-3’

Seq4mmC. 5’-ACTTCTCTGCTAGGCTGCTCATGATTGCGTTACTTCA-3’

Seq4mmT. 5’-ACTTCTCTGCTAGGCTGCTCATGATTGCGTTATTTCA-3’

5.2 Preparation of DNA-crosslined nanoparticle aggregates

For a typical photoswitching experiment, 600 μL of solution containing azobenzene-modified DNA-AuNP aggregates was placed inside a stirring cuvette (Starna Cells). The aggregates were formed by mixing equal amounts of Seq1Azo-AuNPs and Seq2-AuNPs for at least 4 h at room temperature. For the 3-strand motif, a volume of 300 μL of Seq3-AuNP solution was first combined with 3 μL 10^{-5} M Seq4 linker (or Seq4mmA, Seq4mmC, Seq4mmT), annealed at 45-50 ˚C, and then incubated at 25 ˚C for ≥ 4 h followed by the addition of 300 μL of Seq1Azo-AuNPs at room temperature. The melting temperature for Seq1Azo-AuNP + Seq2-AuNP is 61.7 ºC and that of Seq1-AuNP + Seq2-AuNP is 52.1 ºC (in 0.01 M PBS, 0.1 M NaCl and 0.01% SDS). Values were determined with extinction-based melting curves using the Agilent 8453 UV-Vis spectrometer, and Tm points were obtained with its built-in denaturalization mode. The temperature ramp starts at 25 ˚C and ends at 75 ˚C with 1 ˚C temperature steps and 2 min hold time.

5.3 Photoswitching azobenzene-modified DNA-AuNP aggregates in solution

The photoswitching setup consists of an LED light source, an aluminum block (with light accessible windows) as a thermal mass holding the quartz cuvette, and a temperature-controlled stirring plate with a thermocouple inserted into the Al block. (Figure 5.1) It was verified that the cuvette solution temperature was the same as the thermocouple setpoint. The UV LEDs (UVTOP325HS) were purchased from Sensor Electronic Technology, Inc. and blue LEDs (Rebel 7, 470 nm) fitted with Optics Lens (Polymer Optics 264 7 Cell Cluster 12° Diffused Optic® array) were obtained from LuxeonStar®. Typically, 4 UV LEDs at ~7 cm away from the cuvette were aligned to give a total power of 0.83 mW/cm^2, as measured by a calibrated Si photodiode. Blue LEDs gave uniform illumination at 11 mW/cm^2.

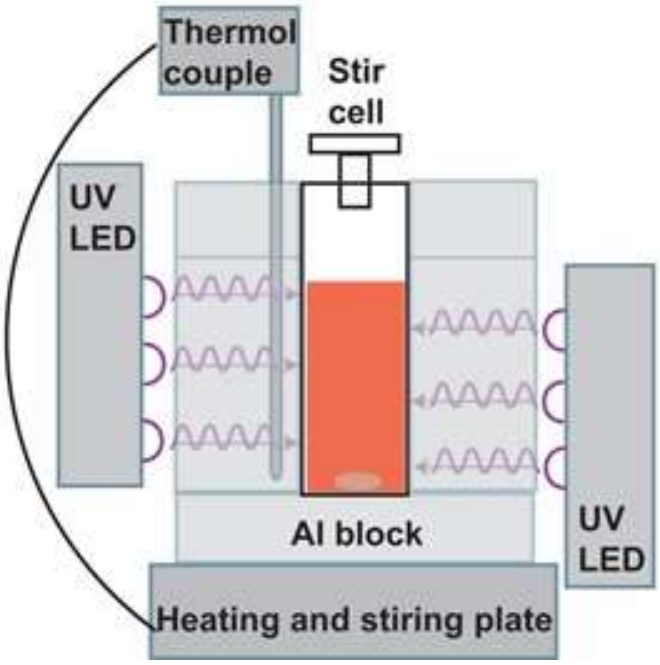

Figure 5.1 Schematic showing the photoswitching set-up.

The azobenzene-modified DNA-functionalized nanoparticle solution, with the stirring bar, sits in the cuvette in the center of the aluminum block. The plate underneath it provides temperature and stirring controls. The LEDs illuminates the sample from both directions.

Prior to any irradiation, the sample was thermally equilibrated for at least 15 minutes. For Seq1Azo-AuNPs and Seq2-AuNPs in 0.01 M PBS, 0.1 M NaCl and 0.01% SDS, photoswitching was performed at 45^{o} C. For discriminating between different Seq4 linkers, photostringency was performed at 30 ^{o}C in 0.01 M PBS, 0.05 M NaCl and 0.01% SDS. UV-vis spectra of the solution were taken with an Agilent 8453 diode array spectrophotometer.

5.4 Photoinduced dissociation study with the dark field microscope

Dr. Jennifer Chen contributed to the measurement and data analysis. I learned and assisted her with the microscope setup and sample preparation.

The azobenzene-modified DNA-linked nanoparticle aggregates were prepared as described in section 5.1(2). About 5-10 μL of the nanoparticle aggregates solution was dropped on the 1-inch-by-1-inch microscope coverslip whose surface was coated with 3-aminopropyltrimethoxysilane. We let the solution sitting on the coverslip surface for ~10-20 min, and then we rinsed the solution with phosphate buffer solution and 0.3M ammonium acetate solution before drying it with nitrogen. The area on the coverslip where the aggregates deposited was immediately covered with phosphate buffer (0.01 M PBS, 0.1 M NaCl and 0.01% SDS) using a sealed hybridization chamber (SecureSeal^{TM} SA8R, Grace Bio-Labs). The nanoparticle sample stayed in the buffer during the UV irradiation and data acquisition process.

We used the Nikon TE-2000 inverted microscope coupled with a transmitted darkfield condenser and a color CCD camera (Diagnostic Instrument, FX1520) to obtain the scattering images of the azobenzene-modified nanoparticle system.(Figure 5.2c) A total magnification of 75X was reached by using a 50X objective lens and an intermediate 1.5X lens. The tungsten halogen lamp provides light to illuminate the sample after passing through the darkfield condenser, which created the darkfield scattering images. The intense white light from the metal

halide lamp and the 375±10-nm optical filter together served as the UV irradiation source. After the filter, the UV light beam was focused by the objective lens to a micrometer-sized spot on the glass surface, and the UV intensity was varied to be 0.25-1.8 W/cm^2. The sample stage was mounted with a home-made copper plate for temperature control.

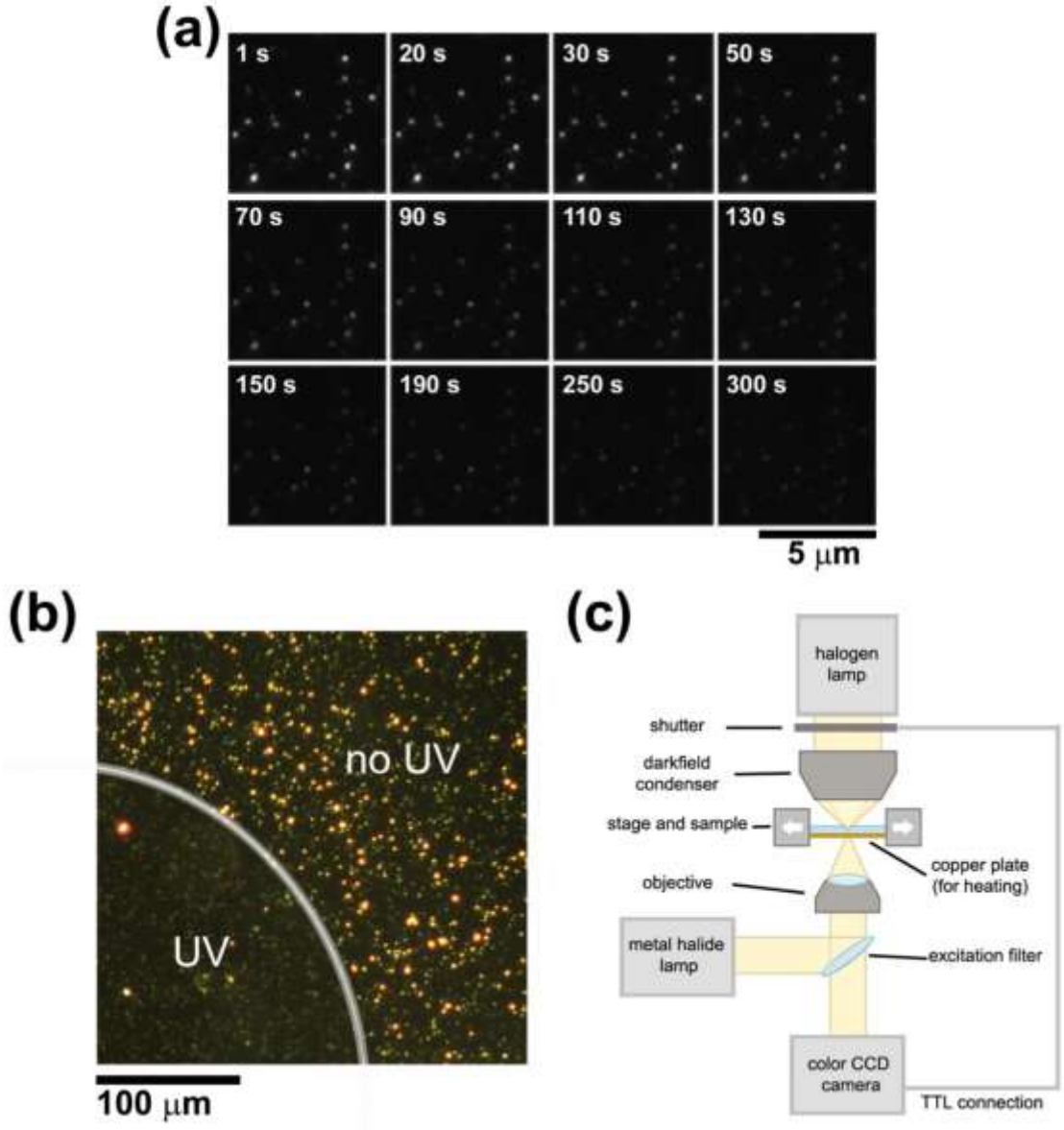

Figure 5.2 Darkfield microscopy data of photoinduced disaggregations of anchored gold nanoparticles.

(a) Darkfield images of aggregates on a substrate at different duration of UV irradiation (with intermittent exposure to darkfield light when images were captured). (b) Darkfield image at low magnification showing an area that had been UV irradiated vs an area without irradiation at same temperature. (c) Schematic showing the microscope setup.

The sample was exposed to the UV irradiation for a total of 8-16 min while a series of black-and-white images were captured by the CCD camera.(Figure 5.2a) However, the sample was briefly exposed to another light source (which gives rise to the darkfiled scattering images) for 106 ms, with a total exposure time being 2-6 s considering all images that were taken. About 30-40 individual white spots in a single image were calculated and the corresponding average intensity was reported for that irradiation time. Figure 5.2b is a darkfield image with lower resolution, showing that the UV area is dimmer than non-UV area. It proves that it was the UV irradiation that caused the dissociation of nanoaprticle aggregates, because both areas were kept under same conditions otherwise.

5.5 Discussions on photothermal effect

I calculate the *maximum* energy from UV and blue LEDs absorbed by single AuNPs. Note that the extinction of the aggregated solutions is actually lower than for the dispersed single AuNPs; hence the value calculated here is an overestimate. From Figure 2.2b, dispersed single AuNPs exhibit an extinction of 1.14 at wavelength 330 nm and 0.978 at wavelength 470 nm, corresponding to absorption of 93 % of the UV and 90 % of the blue light, respectively (scattering is negligible for 15 nm-diameter AuNP). Based on the amount of absorption, the intensity of the LEDs and the illumination area on the sample (0.601 cm^2), the particles absorb 1.7 J of UV light after 1 h and 42 J of blue light *after 2 h irradiation* under the conditions we employed in our experiments. These energies are substantially lower than what is typically required for photothermal melting.

Additionally the temperature increase on the surface of an individual nanoparticle in aqueous solution has been derived by Baffou *et al*[2] where

$$\Delta T = \frac{\sigma_{abs} I}{4\pi R_{eq} \beta \kappa_{water}}$$

σ_{abs} is the absorption cross section (m^2), I is the light intensity (W/m^2), R_{eq} is the radius of a sphere (m), β is the thermal capacitance coefficient (1 for spherical particles), and κ_{water} is the thermal conductivity of water (0.6 W/m*K). For gold nanoparticles with $\sigma_{abs} \sim 10^{-15}$ m^2,[3] the temperature changes upon exposure to 330 nm UV light at the power used here are 1.5×10^{-7} K, and 1.9×10^{-6} K for blue (470 nm) light. The negligible heating strongly argues against photothermal heating as the disassembly mechanism, as confirmed by the native DNA (without azobenzene modification) controls. Furthermore, the more intense blue LED causes hybridization and aggregation in our experiment, while the lower powered UV LED causes melting. Hence the assembly process agrees with photoisomerization-controlled melting mechanism.

5.6 Preparing azobenzene-modified DNA solution for quantum yield measurements

(1) Materials

Unmodified DNAs and azobenzene-modified DNAs were purchased from Integrated DNA Technology (IDT Inc, IA). All sequences used are shown in Table 3.1. Water was deionized to 18.0 MOhm with the Millipore filtration system.

(2) Preparation of dsDNA solution

Aliquots of lyophilized DNA were dissolved in water and a desired amount of DNA aqueous solution was then brought to 0.01M phosphate buffer (pH=6.5), 0.1M NaCl and 0.02% sodium azide. Equal moles of complementary DNAs were mixed at room temperature and

annealed at 95 ˚C for 5 min. The concentration[4] of azobenzene modified dsDNA for quantum yield tests was prepared to be 10 μM; and the concentration for T_m test was 2 μM. The dsDNA solution was kept at 4 ˚C before use.

(3) Preparation of the dsDNA that has three-sequence structure

The sequences for the three-strand capture assay are shown in Figure 3.6(a). Sequence-1 and Sequence-2 are both complementary to part of Sequence-3. The annealing process consisted of two steps. First, Sequence-2 and Sequence-3 were combined and annealed at 95 ˚C for 5 min, followed by gradual cooling to 55 ˚C and being held at 55˚C for 30 min. Then, Sequence-1 was added to the solution and annealed for an additional 10 min at 55 ˚C. The DNA solution was lowered to room temperature and kept at 4 ˚C before use.

5.7 Photoinduced isomerization quantum yield measurement

The UV irradiation setup for quantum yield measurement consisted of an LED light source centered at 330 nm with FWHM less than 10 nm (UVTOP325HS Sensor Electronic Technology, Inc.), a home-made aluminum stage, a quartz cuvette with 1 cm optical path length, a stir plate, and a temperature controller. The temperature of the DNA solution as a function of temperature controller set point (measured in the aluminum stage) was calibrated using a thermometer. The temperature of the DNA solution was kept at 28 ˚C for all quantum yield measurements using the calibrated temperature controller. The UV LEDs were warmed up for 1 h and then the illumination intensity was monitored using a silicon photodiode positioned at the other end of the aluminum stage. The UV intensity was typically 0.37 to 0.42 mW/cm^2. Azobenzene-modified DNA solutions were added to the quartz cuvette and were thermally equilibrated at 28 ˚C for 1 h in the dark before UV irradiation. During UV irradiation, UV-vis absorption spectra were recorded by an Agilent 8453 UV-vis spectrometer every 1 min for 15

min and then every 5 min for the rest 45 min. The DNA solution was stirred during the measurement. We verified that the low intensity white light source of the spectrometer had no significant effect on the photoisomerization process.

5.8 Quantum yield calculation methods

The azobenzene *trans*-to-*cis* isomerization quantum yield is the ratio between the number of isomerized *trans*-azobenzenes and that of absorbed photons at the actual time (a differential quantum yield). We use the following isomerization rate equation:

$$\frac{d[cis]_t}{dt} = \frac{I*l*\left(1-10^{-abs(t)}\right)*\phi_{trans}*\varepsilon_{trans}}{V*abs(t)}\left([trans]_0 - [cis]_t\right) - \frac{I*l*\left(1-10^{-abs(t)}\right)*\phi_{cis}*\varepsilon_{cis}}{V*abs(t)}[cis]_t$$

Equation 1

where $[cis]_t$ is the concentration of *cis*-azobenzene at time t; $[trans]_0$ is concentration of *trans*-azobenzene before photoisomerization which we assume to be the total concentration of azobenzene; I is the intensity of the excitation; l is the beam path length of UV-vis absorption measurement; $abs(t)$ is the absorbance of the sample at the excitation wavelength, and t is time; ϕ_{trans} and ϕ_{cis} are the quantum yields of *trans*-to-*cis* and *cis*-to-*trans* isomerization; ε_{trans} and ε_{cis} are the absorption coefficients at the excitation wavelength of *trans*-azobenzene and *cis*-azobenzene; V is the volume.

The left side of the equation 1 describes how fast cis-azobenzene is produced by quantifying the cis-azobenzene concentration change against time. On the right side of the equation, the first term corresponds to how fast the trans-azobenzene isomerizes to the cis-azobenzene, which contributes positively to the production of cis-azobenzene; the second term on the right side corresponds to how fast cis-azobenzene isomerizes to the trans-from, which contributes negatively to the production of cis-azobenzene.

The term "$I * \left(1 - 10^{-abs(t)}\right)$" corresponds to the amount of light being absorbed by the whole system; the term "$\varepsilon_{trans} * l * ([trans]_0 - [cis]_0)$" corresponds to the light absorption of the trans-azobenzene, while "$abs(t)$" is light absorption of the total system measured by the device; a ratio of the multiply by the amount of light absorbed by the system (($I * \left(1 - 10^{-abs(t)}\right) * \frac{\varepsilon_{trans} * l * ([trans]_0 - [cis]_0)}{abs(t)}$) gives rise to the total amount of light absorbed only by the trans-azobenzene, which gives rise to the number of trans-azobenzene consumed by multiplying with the trans-to-cis quantum yield $\left(1 - 10^{-abs(t)}\right) * \frac{\varepsilon_{trans} * l * ([trans]_0 - [cis]_0)}{abs(t)} * \phi_{trans}$). Doing similar to the second term on the right side, cis-to-trans quantum yield is included in the equation; the rest is to solve the equation.

Since $\frac{d[cis]_t}{dt} = 0$ at the photostationary state, we get the following relation

$$\frac{\phi_{trans}}{\phi_{cis}} = \frac{[cis]_\infty * \varepsilon_{cis}}{([trans]_0 - [cis]_\infty) * \varepsilon_{trans}}$$

Equation 2

where $[cis]_\infty$ is the concentration of *cis*-azobenzene at photo-stationary state. By defining the fraction of *cis*-azobenzene as $y = \frac{[cis]}{[trans]_0}$ and the fraction of *trans*-azobenzene as $1 - y$, and by solving Equation 1 and 2, we obtain the following equation

$$\ln \frac{y_\infty - y}{y_\infty - y_0} = -\frac{I * l * \phi_{trans} * \varepsilon_{trans}}{V * y_\infty} \int_{t_0}^{t} \frac{1 - 10^{-abs^\lambda(t)}}{abs^\lambda(t)} dt$$

Equation 3

By replacing $\frac{I * l * \phi_{trans} * \varepsilon_{trans}}{V * y_\infty}$ as pre-factor A, and $\int_{t_0}^{t} \frac{1 - 10^{-abs^\lambda(t)}}{abs^\lambda(t)} dt$ as variable x, we obtain Equation 4 shown below

$$y = (y_0 - y_\infty)\exp(-Ax) + y_\infty$$

Equation 4

As described in the chapter 3, y value (the fraction of cis-azobenzene) is plotted against x value and quantum yield is calculated after A value is extracted from the curve fitting. The term $x(t) = \int_0^t \frac{1-10^{-abs(t)}}{abs(t)} dt$ an integration of photokinetic factor.

5.9 DNA melting temperature measurements

An Agilent 8453 UV-vis spectrometer operating in the thermal denaturation mode was used to measure the melting temperature. The temperature ramp started at 5 ˚C and ended at 95 ˚C with 2 ˚C step interval and a 5 min hold time. Melting temperature was determined as the temperature at which the first derivative of the absorbance vs. temperature plot was maximum. (Figure 5.3)

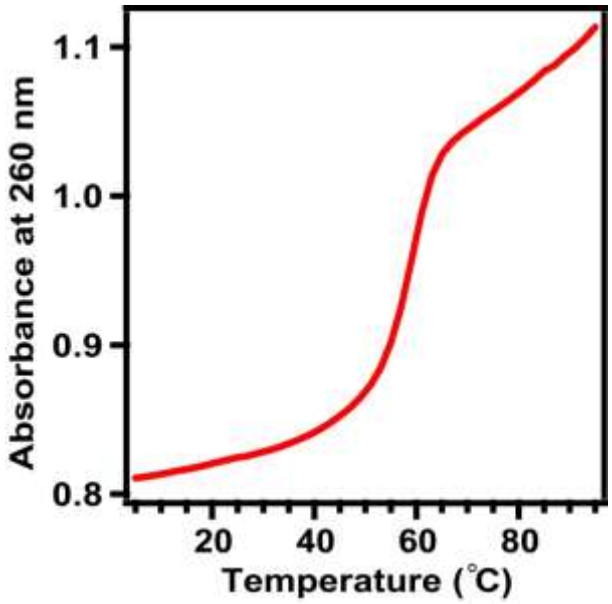

Figure 5.3 An example plot of the absorbance at 260 nm as a function of temperature to obtain the melting temperature (T_m) of azobenzene-modified dsDNA.

The T_m is determined as the temperature at which the first derivative of absorbance against temperature is the largest. The plot shown here corresponds to the dsDNA of Seq-complement with T_m equals to 60 ˚C.

5.10 Preparation of DNA immobilized glass substrates

I adapted the method from O'Ferral et al to covalently attach thiol oligonucleotides to glass substrates.[5] Briefly, plain glass microscope slides were purchased from Fisher Scientific, and cleaned by 15 min sonication in isopropyl alcohol and 5 min exposure to air plasma. Glasses were then modified with an amino monolayer via reaction in 1% (v/v) 3-aminopropyltriethoxysilane ethanoic solution for 20 min at room temperature. Soon after, glasses were annealed at temperature of ~95-100 °C for 5 min. Hetero-bi-functional succinimidyl 4-[malemido-phenyl]butyrate (SMPB, 10 mM in 1:4 DMSO:ethanol solution) was added onto glass substrates immediately after heating and was kept for 2 hr at room temperature. Newly cleaved 0.5 µL10 µM thiolated DNA was quickly dropped onto glass substrates using a digital pipette; each glass had 8 drops and was kept at 40%-50% humidity for 2 hr at room temperature. After DNA attachment, substrates were submerged in 1x SSPC buffer for 5 min; then glass substrates were dried and stored at room condition. Modified substrates were used within one week.

I followed instructions from Arrayit Cooperation to covalently attach amino-terminated oligonucleotides onto substrates. The glass substrates (SuperAmine slides, SME2, Arrayit) were already modified with epoxy groups. Newly prepared 0.5 µL 10 µM amino oligonucleotide in Micro Spotting Solution Plus (MSP, Arrayit) was kept on SuperAmine slides overnight. Slides were then rinsed with deionized water and stored at room condition. Right before usage, slides were pre-treated with BlockIt blocking buffer (BKT, Arrayit) for 1 hr followed by multiple wash steps.

5.11 Hybridization of the immobilized DNA substrates

Glasses immobilized with DNA spots were sealed with a SecureSeal^{TM} hybridization chamber (#621503, Grace Bio-Labs) before adding the target DNA solution. Figure 5.4 depicts the DNA sequences used for the experiment and the outline of hybridization chamber. Hybridization happened at a controlled elevated temperature, but below the melting temperature of to-be-formed double-stranded DNA. After 2-hour hybridization, the glass was immediately exposed to 365 nm home-made UV LED assembly (LZ4-00U600, LED Engine). After UV irradiation, the hybridization chamber was peeled off by hand and the microarray glass was rinsed with 4 °C 20 mM phosphate buffer silane solution. The glass was then scanned.

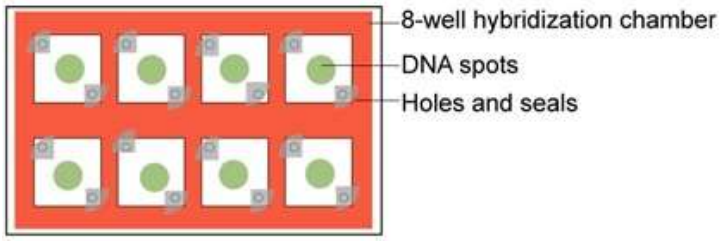

Figure 5.4 Schematic of DNA sequences used in the azobenzene-modified DNA chip experiment.

The diagram of DNA microarrays in the hybridization and photo-induced de-hybridization experiments. The glass array was covered with an 8-well hybridization chamber, whose cell holes were able to be sealed. The green dot at the center of each cell had spotted DNA molecules.

5.12 Fluorescent scanning

A fluorescent scanner (Typhoon^{TM} FLA 9000, GE Healthcare) was used to excite the "substrate" fluorophores linked on target DNA and to obtained images at the same time. The linked fluorophore is tetramethylrhodamine, and the excitation source was a 532-nm laser, and the scanning pixel resolution was set at 50 μm.

5.13 References

(1) Hurst, S. J.; Lytton-Jean, A. K.; Mirkin, C. A. *Anal Chem* **2006**, *78*, 8313-8318.

(2) Baffou, G.; Quidant, R.; Garcia de Abajo, F. J. *ACS Nano* **2010**, *4*, 709-716.

(3) Jain, P. K.; Lee, K. S.; El-Sayed, I. H.; El-Sayed, M. A. *J Phys Chem B* **2006**, *110*, 7238-7248.

(4) Nishioka, H.; Liang, X.; Kato, T.; Asanuma, H. *Angew Chem Int Ed Engl* **2012**, *51*, 1165-1168.

(5) Chrisey, L. A.; Lee, G. U.; O'Ferrall, C. E. *Nucleic Acids Res* **1996**, *24*, 3031-3039.

Chapter VI. Conclusions and Future Work

6.1 Conclusions

The dissertation includes photochemical studies of azobenzene-modified DNA with the purpose to pursue applications of light-controlled hybridization stringency with gold nanoparticles and DNA-immobilized chips. Chapter 2 describes the construction of photoswitchable gold nanoparticle materials that are heavily functionalized with azobenzene-modified oligonucleotides. Nanoparticle solutions have exhibited reversible color and structural change with alternate UV and blue irradiations caused by the photoinduced hybridization and dehybridizaiton of azobenzene-modified DNA. In addition to heat- and salt-controlled hybridization stringency, photo-controlled hybridization stringency has been discovered that DNA duplexes with partially matched sequences dehybridize more rapidly under light than that of perfectly-matched sequences.

Further effort has been spent to study the photochemical kinetics and photoisomerization quantum yield of azobenzene-modified DNA. Chapter 3 shows that the isomerization quantum yield of azobenzene-modified DNA has decreased by 3-fold to 15-fold compared to that of free azobenzene that is not functionalized with DNA. However, for azobenzene-modified DNA, the quantum yield increases when the duplex has the single-base-mismatched pair, and rises further when the mismatched pair is immediately next to the azobenzene. Control experiments exclude the impact of electronic interactions, proving that the quantum yield variation depends on DNA sequences.

Last part of the dissertation presents studies of covalently attaching azobenzene-modified oligonucleotides on glass slides with the goal to pursue chip-based applications for photonic hybridization stringency. Chapter 4 demonstrates that immobilized azobenzene-modified DNA is

compatible with surface fluorescent detection, opening opportunities for azobenzene-modified DNA in a variety of chip-based applications with fluorescent readout. Controlling DNA hybridization stringency with light has been achieved on DNA arrays in this chapter, expanding the possibilities to apply photonic hybridization stringency to heterogeneous array applications.

The appendix A describes a chemical approach to synthesize nanoparticle dimers from DNA-functionalized nanoparticles without additional surface modifications or purifications. Collaborating with Dr. Lucas Parents and Dr. James Evans at pacific northwestern national laboratory, we used liquid TEM cells to capture motions of dimer nanoparticles in aqueous buffer in order to independently and directly calculate/calibrate the interparticle distance of DNA-linked dimers.

Results in chapter 2-4 have been published or ready for publication; and results in appendix A is preliminary with comments for future directions below.

6.2 Future Work

(1) Applications of photonic hybridization stringency

It is demonstrated in chapter 2 that azobenzene-modified DNA-functionalized nanoparticles have allowed photonic energy to control DNA hybridization stringency with the ability to detect a single base difference in the sequence. Chapter 4 shows that one can achieve photonic hybridization stringency on DNA immobilized substrates. With either platform, it would be worth to use photonic hybridization stringency to detect a nucleic acid sequence of interest; which would require literature search to design target and probe sequences. A further to-do test is to assess the photonic hybridization stringency through side-by-side comparison with heat- and salt-induced stringency in single base mismatch detection.

(2) Temperature dependence of quantum yield

Chapter 3 discovers that the photoisomerization quantum yield of azobenzene-modified DNA depends on DNA sequences as well as the DNA melting temperature. We have proposed the "free volume" hypothesis to explain the phenomenon that photoisomerization quantum yield is suppressed when the mismatched base pair is further away from the azobenzene. As increasing temperature would destabilize the duplex which could result in more "free volume" around the azobenzene, I would predict an increase in azobenzene quantum yield with increased environmental temperature. Chapter 3 describes the dependence of quantum yield on the melting temperature for different sequences, and the next step is to uncover the dependence of quantum yield on temperature for azobenzene-modified sequences.

We have started the collaboration with Prof. Lutz Maibaum to further understand the sequence-dependent quantum yield of azobenzene-modified DNA using molecular dynamic simulations. We would support and assess the simulation methods by designing azobenzene-modified sequences and measuring experimental quantum yield values.

(3) Complete interparticle-distance measurement with liquid TEM

I would propose the continued collaboration with the liquid TEM experts to acquire more data of DNA-linked nanoparticle dimers, in order to calibrate the interparticle distance as a function of sequence length and particle size.

Appendix A. Measuring the interparticle distance by using in-situ liquid TEM

Introduction

Gold nanoparticles, which are heavily functionalized with DNA, have been widely studied for applications ranging from biological and chemical sensing[1] to programmable assembly of 3-D crystals.[2,3] These applications rely on constructions of metal nanoparticles in well-defined structures in order to exhibit unique plasmonic features that are sensitive to the interparticle distance. For example, plasmon rulers[4] are constructued with DNA-functionalized nanoparticles to measure distance change in sub-nanometer range by monitoring of the plasmonic peak shift. In order to calibrate and assess the accuracy of plasmon ruler materials, I study to develop an independent method that can measure the interparticle distance with a distinct mechanism.[5]

Researchers have used small angle X-ray scattering (SAXS) technique,[6-8] cryo TEM[9] and theoretical simulations[10] to independently measure the interparticle distance of nanoparticle structures that are created with DNA modified nanoparticles. SAXS can only provide ensemble average values of concentrated nanoparticle sample; and it neglects the particle shape by assume particle being spherical. Cryo TEM loses the information of interparticle distance in dynamic bio-environment because it can only measure frozen particles. To overcome these limitations, I explore to utilize liquid-enabled TEM to measure the interparticle distance by capturing the motion of nanoparticles in-situ.

Liquid TEM, though operated under extreme vacuum, can allow direct visualization of aqueous DNA-linked nanomaterials by using a special sample holder that completely seals the liquid in a micro-chamber.[11] TEM captures one video of nanoparticle materials that consist of thousands of projected frames. Each frame is a two-dimensional projected image that is processed

to calculate the interparticle distance. The free motion of nanoparticles in buffer gives particles the opportunity to reach the same focal plane at the same time during the video period. It results in a plot of interparticle distance versus frame number (time), in which the largest distance is considered the interparticle distance in aequous buffer.

The liquid TEM instrument locates at Pacific Northwestern National Laboratory. The experiment is collaborated with graduate student Lucas Parent and with staff scientist James Evans. I prepare the nanoparticle solutions and analyze the TEM video data. Lucas and James operates the TEM to obtain the video data.

Synthesis of nanoparticle dimers

The nanoparticle structure in our measurement consists of two gold nanoparticles (referred as "dimer") with different sizes that are linked by dsDNA. Scheme A-1 shows the preparation method. It starts by mixing two types of gold nanoparticles—the larger nanoparticles functionalized with sequence A and the smaller particles functionalized with sequence B. Through hybridization of sequence A and B, bigger particles and smaller particles are cross-linked to form structures such as dimer, trimer (that have three particles), multimer (that have more than three particle) and even larger clusters. In order to make dimer, the quenching DNA is added in the mixed solution to stop the nanoparticles from growing larger in size because the quenching DNA will form duplex DNA with sequence A. To obtain a solution with highest possible number of dimer and lower possible number of larger clusters, the quenching DNA needs

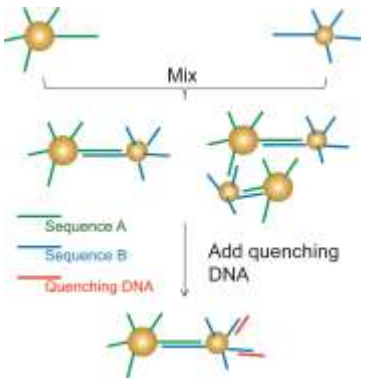

Scheme A-1. Preparation method of dimers. DNA modified nanoparticles with two different sizes are mixed. Quenching DNA is added, after mixing, to stop the nanoparticles from growing into large clusters.

to be added at the right time. Therefore, we study the change in dimer's yield while varying the length of time nanoparticles are mixed before quenching DNA is added.

The dimer's yield is calculated by counting the ratio between the number of dimers and the total number of particles with varied structures. The scanning electron microscope (SEM) is used to take images of the prepared nanoparticle solution. Figure A-2(a) shows one example of SEM images of the sample with 30 nm and 15 nm gold nanoparticles functionalized with 90-base-long DNA. In this image, the number of dimer is 33, and total number of particles is 150, so the dimer's yield is 0.22. To report a reliable dimer's yield, the total number of particles counted must exceed 1000. Figure A-2(b) shows the plot of dimer's yield and other structures' yields versus the length of mixing time for the sample of 30 nm and 15 nm nanoparticles attached with 90-base-pair long DNA. The plot indicates that as mixing time increases, dimer's yield, trimer's yield, larger cluster's yield all increase while yields of single nanoparticles decrease; the plot suggests an optimal mixing time of 15 min because it leads to a higher dimer's yield and lower cluster's yield. Figure A-2(c) plots dimer's yield versus mixing time for different nanoparticle samples (red for 30 nm and 15 nm with 90-base-pair DNA, green for 100 nm and 60 nm with 90-base-pair DNA,

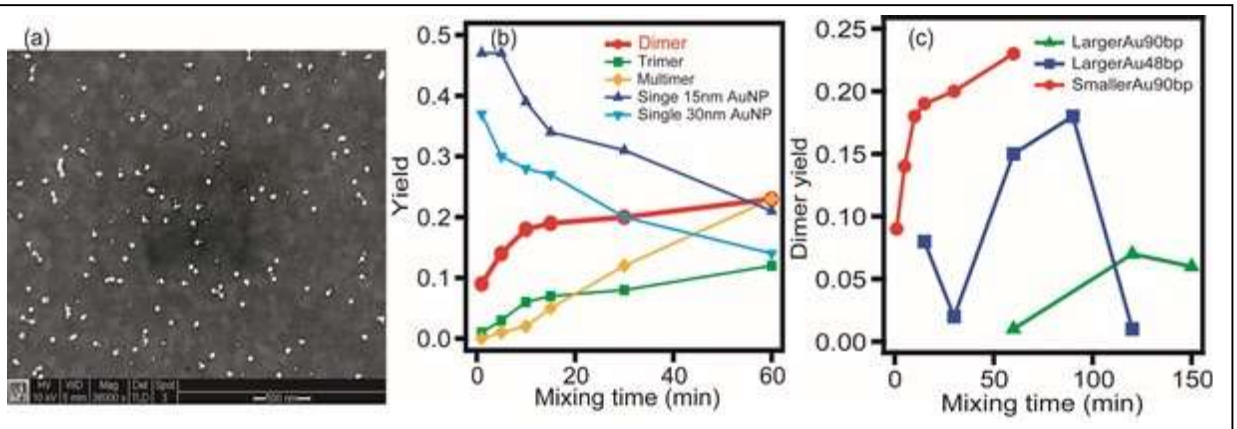

Figure A-2. The result of dimers prepared in solution. (a) An example of one SEM image of the nanoparticle solution that is used to count the number of clusters. (b) The yield of dimer, trimer, multimer and single nanoparticles versus mixing time before quenching DNA is added. (c) The yield of dimer versus mixing time. The dimer is prepared by using nanoparticles with varied sizes and DNAs with varied length

and blue for 100 nm and 60 nm with 48-base-pair DNA). It indicates, in this plot, that relation between dimer's yield and mixing time depends on the sizes of nanoparticles and the base-length of DNAs that are attached on these nanoparticles. Dimer's yield reaches the highest at 1 hour for red, and 2 hour for green, and 1.5 hour for blue. It suggests that the larger the size of nanoparticles and the longer the linked DNA, the longer the mixing time will be.

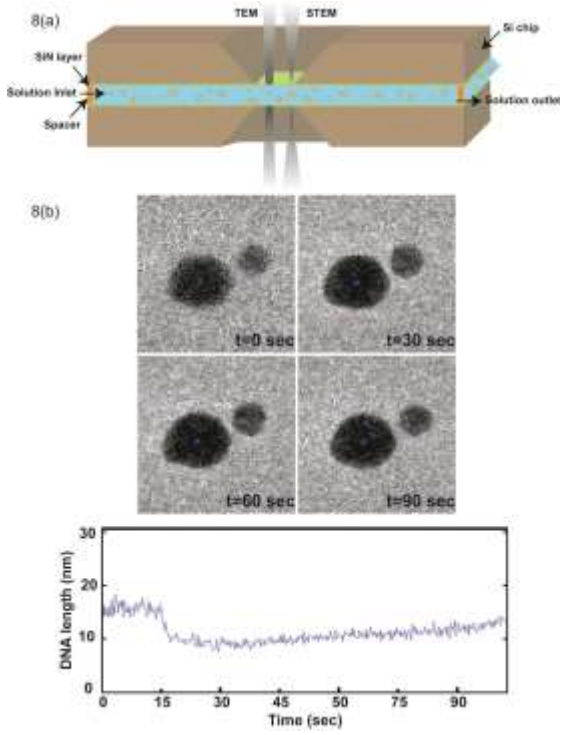

Figure A-3 (a) The diagram of liquid TEM. The liquid sample is sandwiched between two silicon chip. The window in the center allows electrons to travel through to generate TEM images. (b) An example of analyzing TEM video to get interparticle distance. The pictures are frames of the video at different time points. The interparticle distance is measured in each frame and plotted versus time.

The interparticle distance of dimers formed by 60 nm and 100 nm nanoparticles with 90-base-pair DNA is measured using the liquid TEM study. The solution is sandwiched between two silicon TEM chips, with a 50 μm by 50 μm viewing window for electron beam to pass through (Figure A-3(a)). The free movement of dimer is capture by a CCD video for known time. Each frame of this video is analyzed to firstly locate the centroids of two nanoparticles, and secondly calculate the interparticle distance, and lastly calculate the distance per base pair. Figure A-3(b) shows video frames of nanoparticles at different time points and the plot of interparticle distance versus time. The dimer exhibits its longest interparticle distance as 18 nm, and shortens its interparticle distance after that time point. The distance of each base pair is 0.2 nm, taking into account the duplex DNA has 90 base pairs. The longest distance of the dimer is obtained when two nanoparticles are in the same focal plane.

The dimers need good mobility in solution so that its longest interparticle distance has a higher chance to be captured when two particles have a higher chance to rotate into the sample focal plane. The hypothesis explains why dramatically differently distances

Conclusion

Liquid TEM is used to measure the interparticle distance of dimers made of DNA modified gold nanoparticles. The interparticle distance is 18 nm for a 60 nm and 100 nm dimer with 90-base-pair DNA, which leads to a length of 0.2 nm per base pair.

Proposed Research

The preliminary data shown in Figure A-2(b) and A-2(c) demonstrate the option and limitations of using liquid TEM to measure interparticle distance of DNA-linked dimers in buffer solution. To improve this method, I propose the following experiments.

(1) Repeating dimer preparation and liquid TEM experiments to obtain the errors of interparticle distance measurement;

So far, we measured reliable interparticle distance from four dimer samples. As the interparticle distance value varies a lot from sample to sample, I have not obtained a reliable error value. So, I seek to repeat the experiments and measure more dimers to get the idea of the error of liquid TEM method.

(2) Measuring interparticle distance of dimers that are made of particles with different size and DNAs with different length;

I only measured the interparticle distance of dimers that are made of 60 nm and 100 nm gold nanoparticles and DNA with 90-base-pair length. DNA length has an effect on the flexibility of dsDNA, and thus has an effect on the interparticle distance because two nanoparticles are linked

by dsDNA. The size of the particles may also have an effect on interparticle distance. I seek to find out these effects.

(3) Attaching nanoparticles on TEM chip to achieve more dimers under TEM view;

Given the size of the TEM viewing window (2.5E-12 L) and the concentration of nanoparticle solution (~0.01-0.1 nM for 100 nm and 60 nm particles), the theoretical number of dimer one can detect in the view is 1 – 3 (20% dimer's yield). To achieve more dimers in the view, I seek to chemically attach one nanoparticle on the TEM chip, and let the other nanoparticle attach to the substrate nanoparticle and stay free in solution.

(4) Studying in-situ photoswitching of dimers

The liquid TEM instrument at Pacific Northwestern National Laboratory is going to be launched with laser pulse which can send the light trigger into the sample while watching the effect of the trigger. In conjunction with the photoswitchable nanoparticle experiments, I propose to photoswitch DNA linked nanoparticle clusters in solution inside the liquid TEM chamber and study the photoswitching process in situ.

References

(1) Rosi, N. L.; Mirkin, C. A. *Chemical Reviews* **2005**, *105*, 1547-1562.

(2) Park, S. Y.; Lytton-Jean, A. K. R.; Lee, B.; Weigand, S.; Schatz, G. C.; Mirkin, C. A. *Nature* **2008**, *451*, 553-556.

(3) Nykypanchuk, D.; Maye, M. M.; van der Lelie, D.; Gang, O. *Nature* **2008**, *451*, 549-552.

(4) Sonnichsen, C.; Reinhard, B. M.; Liphardt, J.; Alivisatos, A. P. *Nature Biotechnology* **2005**, *23*, 741-745.

(5) Reinhard, B. M.; Siu, M.; Agarwal, H.; Alivisatos, A. P.; Liphardt, J. *Nano Letters* **2005**, *5*, 2246-2252.

(6) Park, S. J.; Lazarides, A. A.; Storhoff, J. J.; Pesce, L.; Mirkin, C. A. *Journal of Physical Chemistry B* **2004**, *108*, 12375-12380.

(7) Mastroianni, A. J.; Sivak, D. A.; Geissler, P. L.; Alivisatos, A. P. *Biophysical Journal* **2009**, *97*, 1408-1417.

(8) Chi, C.; Vargas-Lara, F.; Tkachenko, A. V.; Starr, F. W.; Gang, O. *Acs Nano* **2012**, *6*, 6793-6802.

(9) Lermusiaux, L.; Sereda, A.; Portier, B.; Larquet, E.; Bidault, S. *Acs Nano* **2012**, *6*, 10992-10998.

(10) Jain, P. K.; Huang, W. Y.; El-Sayed, M. A. *Nano Letters* **2007**, *7*, 2080-2088.

(11) Parent, L. R.; Robinson, D. B.; Woehl, T. J.; Ristenpart, W. D.; Evans, J. E.; Browning, N. D.; Arslan, I. *Acs Nano* **2012**, *6*, 3589-3596.